A NEW FRAMEWORK FOR TENSOR PCA BASED ON TRACE INVARIANTS

Anonymous authors
Paper under double-blind review

ABSTRACT

We consider the Principal Component Analysis (PCA) problem for tensors $\mathbf{T} \in (\mathbb{R}^n)^{\otimes k}$ of large dimension n and of arbitrary order $k \geq 3$. It consists in recovering a spike $\boldsymbol{v}_0^{\otimes k}$ (related to a signal vector $\boldsymbol{v}_0 \in \mathbb{R}^n$) corrupted by a Gaussian noise tensor $\mathbf{Z} \in (\mathbb{R}^n)^{\otimes k}$ such that $\mathbf{T} = \beta \boldsymbol{v}_0^{\otimes k} + \mathbf{Z}$ where β is the signal-to-noise ratio. In this paper, we propose a new framework based on tools developed by the theoretical physics community to address this important problem. They consist in trace invariants of tensors built by judicious contractions (extension of matrix product) of the indices of the tensor $\mathbf{T}$. Inspired by these tools, we introduce a new process that builds for each invariant a matrix whose top eigenvector is correlated to the signal for β sufficiently large. Then, we give examples of classes of invariants for which we demonstrate that this correlation happens above the best algorithmic threshold ($\beta \geq n^{k/4}$) known so far. This method has many algorithmic advantages: (i) it provides a detection algorithm linear in time and with only $O(1)$ memory requirements (ii) the algorithms are very suitable for parallel architectures and have a lot of potential of optimization given the simplicity of the mathematical tools involved (iii) experimental results show an improvement of the state of the art for the symmetric tensor PCA. Furthermore, this framework allows more general applications by being able to theoretically study the recovery of a spike in the form of $\boldsymbol{v}_1 \otimes \cdots \otimes \boldsymbol{v}_k$ with different dimensions ($\mathbf{T} \in \mathbb{R}^{n_1 \times n_2 \times \cdots \times n_k}$ with $n_1, \ldots, n_k \in \mathbb{N}$) as well as the recovery of a sum of different orthogonal spikes. We provide experimental results to these different cases that match well with our theoretical findings.

1 INTRODUCTION

Powerful computers and acquisition devices have made it possible to capture and store real-world multidimensional data. For practical applications (Kolda & Bader (2009)), analyzing and organizing these high dimensional arrays (formally called tensors) lead to the well known curse of dimensionality (Gao et al. (2017),Suzuki (2019)). Thus, dimensionality reduction is frequently employed to transform a high-dimensional data set by projecting it into a lower dimensional space while retaining most of the information and underlying structure. One of these techniques is Principal Component Analysis (PCA), which has made remarkable progress in a large number of areas thanks to its simplicity and adaptability (Jolliffe & Cadima (2016); Seddik et al. (2019)).

In the Tensor PCA, as introduced by Richard & Montanari (2014), we consider a model where we attempt to detect and retrieve an unknown unit vector $\boldsymbol{v}_0$ from noise-corrupted multi-linear measurements put in the form of a tensor $\mathbf{T}$. Using the notations found below, our model consists in:

$$\mathbf{T} = \beta \boldsymbol{v}_0^{\otimes k} + \mathbf{Z}, \tag{1}$$

with $\mathbf{Z}$ a pure Gaussian noise tensor of order k and dimension n with identically independent distributed (iid) standard Gaussian entries: $\mathbf{Z}_{i_1, i_2, \ldots, i_k} \sim \mathcal{N}(0, 1)$ and β the signal-to-noise ratio.

To solve this important problem, many methods have been proposed. However, practical applications require optimizable and parallelizable algorithms that are able to avoid the high computationally cost due to an unsatisfactory scalability of some of these methods. A summary of the time and space requirement of some existent methods can be found in Anandkumar et al. (2017).

One way to achieve this parallelizable algorithm is through methods based on tensor contractions (Kim et al. (2018)) which are extensions of the matrix product. These last years, tools based on tensor contractions have been developed by theoretical physicists where random tensors have emerged as a generalization of random matrices. In this paper, we investigate the algorithmic threshold of tensor PCA and some of its variants using the theoretical physics approach and we show that it leads to new insights and knowledge in tensor PCA.

Tensor PCA and tensor decomposition (the recovery of multiple spikes) is motivated by the increasing number of problems in which it is crucial to exploit the tensorial structure (Sidiropoulos et al. (2017)). Recently it was successfully used to address important problems in unsupervised learning (learning latent variable models, in particular latent Dirichlet allocation Anandkumar et al. (2014), Anandkumar et al. (2015)), supervised learning (training of two-layer neural networks, Janzamin et al. (2015)) and reinforcement learning (Azizzadenesheli et al. (2016)).

Related work Tensor PCA was introduced by Richard & Montanari (2014) where the authors suggested and analyzed different methods to recover the signal vector like matrix unfolding and power iteration. Since then, various other methods were proposed. Hopkins et al. (2015) introduced algorithms based on the sum of squares hierarchy with the first proven algorithmic threshold of $n^{k/4}$. However this class of algorithm generally requires high computing resources and relies on complex mathematical tools (which makes its algorithmic optimization difficult). Other studied methods have been inspired by different perspectives like homotopy in Anandkumar et al. (2017), statistical physics (Arous et al. (2020), Ros et al. (2019), Wein et al. (2019) and Biroli et al. (2020)), quantum computing (Hastings (2020)) as well as statistical query (Dudeja & Hsu (2020)).

Recently, a fundamentally different set of mathematical tools that have been developed for tensors in the context of high energy physics have been used to approach the problem. They consist in trace invariants of degree $d \in \mathbb{N}$, obtained by contracting pair of indices of d copies of the tensor $\mathbf{T}$. They have been used in Evnin (2020) to study the highest eigenvalue of a real symmetric Gaussian tensor. Subsequently, Gurau (2020) provided a theoretical study on a function based on an infinite sum of these invariants. Their results suggest a transition phase for the highest eigenvalue of a tensor for β around $n^{1/2}$ in a similar way to the BBP transition in the matrix case (Baik et al. (2005)). Thus, this function allows the detection of a spike. However evaluating it involves computing an integral over a n-dimensional space, which may not be possible in a polynomial time.

The contribution of this paper is the use of these invariant tools to build tractable algorithms with polynomial complexity. In contrast to Gurau (2020), instead of using a sum of an infinite number of invariants, we select one trace invariant with convenient properties to build our algorithms. It lets us detect the presence of the signal linearly in time and with a space requirement in $O(1)$. Moreover, in order to recover the signal vector besides simply detecting it, we introduce new tools in the form of matrices associated to this specific invariant. Within this framework, we show as particular cases, that the two simpler graphs (of degree two) are similar to the tensor unfolding and the homotopy algorithms (which is equivalent to average gradient descent). These two algorithms are the main practical ones known from the point of view of space and time requirement (Anandkumar et al. (2017) provides a table comparison). Interestingly, our framework allows us to go further by using graphs of higher degrees and one can see that the tetrahedral graph (degree four) performs better in the numerical experiments on the symmetric case and gives nearly optimal results for values of n of order 100. We also derive an algorithmic threshold, that is for the best of our knowledge novel and new, that generalizes the threshold $n^{k/4}$ for a spike $\boldsymbol{v}^{\otimes k}$ of a tensor $\mathbf{T} \in \bigotimes \mathbb{R}^n$ to the case of a spike $\boldsymbol{v}_1 \otimes \cdots \otimes \boldsymbol{v}_k$ and $\mathbf{T} \in \bigotimes \mathbb{R}^{n_i}$ where the threshold to recover the vector $\boldsymbol{v}_i$ is given by $\max(n_i^2, (\prod_{i=1}^k n_i))$.

Notations We use bold characters $\mathbf{T}, \boldsymbol{M}, \boldsymbol{v}$ for tensors, matrices and vectors and $\boldsymbol{T}_{ijk}, M_{ij}, v_i$ for their components. $[p]$ denotes the set $\{1, \dots, n\}$. A real $k-$th order tensor is of order k if it is a member of the tensor product of $\mathbb{R}^{n_i}, i \in [k]$: $\mathbf{T} \in \bigotimes_{i=1}^k \mathbb{R}^{n_i}$. It is symmetric if $\boldsymbol{T}_{i_1 \dots i_k} = \boldsymbol{T}_{\tau(i_1) \dots \tau(i_k)}$ $\forall \tau \in \mathfrak{S}_k$ where $\mathfrak{S}_k$ is the symmetric group (more details are provided in Appendix B). For a vector $\boldsymbol{v} \in \mathbb{R}^n$, we use $\boldsymbol{v}^{\otimes p} \equiv \boldsymbol{v} \otimes \boldsymbol{v} \otimes \cdots \otimes \boldsymbol{v} \in \bigotimes^p \mathbb{R}^n$ to denote its p-th tensor power. $\langle \boldsymbol{v}, \boldsymbol{w} \rangle$ denotes the scalar product of $\boldsymbol{v}$ and $\boldsymbol{w}$.

Let's define the operator norm, which is equivalent to the highest eigenvalue of a tensor of any order: $\|\mathbf{X}\|_{\text{op}} \equiv \max \{\mathbf{X}_{i_1, \dots, i_k} (\boldsymbol{w}_1)_{i_1} \dots (\boldsymbol{w}_k)_{i_k}, \forall i \in \{1, \dots, n\}, \|\boldsymbol{w}_i\| \leq 1\}$ The trace of $\boldsymbol{A}$ is

denoted $\mathrm{Tr}(\boldsymbol{A})$. We denote the expectation of a variable X by $\mathbb{E}(X)$ and its variance by $\sigma(X)$. We say that a function f is negligible compared to a positive function g and we write $f = o(g)$ if $\lim_{n\to\infty} f/g \to 0$.

Einstein summation convention It is important to keep in mind throughout the paper that we will follow the Einstein summation convention: when an index variable appears twice in a single term and is not otherwise defined, it implies summation of that term over all the values of the index. For example: $\mathsf{T}_{ijk}\mathsf{T}_{ijk} \equiv \sum_{ijk} \mathsf{T}_{ijk}\mathsf{T}_{ijk}$. It is a common convention when addressing tensor problems that helps to make the equations more comprehensible.

2 General Framework for Signal Detection and Recovery

2.1 What do we use to study the signal?

An important concept in problems involving matrices is the spectral theory. It refers to the study of eigenvalues and eigenvectors of a matrix. It is of fundamental importance in many areas. In machine learning, the matrix PCA computes the eigenvectors and eigenvalues of the covariance matrix of the features to perform a dimensional reduction while ensuring most of the key information is maintained. In this case, the eigenvalues is a very efficient tool to describe data variability. In the case of signal processing, eigenvalue can contain information about the intensity of the signal, while the eigenvector points out to its direction. Lastly, a more theoretical example involves quantum physics where the spectrum of the matrix operator is used to calculate the energy levels and the state associated.

In all of these examples, an important property of the eigenvalues of a n-dimensional matrix $\boldsymbol{M}$ is its invariance under orthogonal transformations $\{\boldsymbol{M} \to \boldsymbol{O}\boldsymbol{M}\boldsymbol{O}^{-1}, \boldsymbol{O} \in \mathrm{O}(n)\}$ where $\mathrm{O}(n)$ is the n-dimensional orthogonal group (i.e. the group of real matrices that satisfies $\boldsymbol{O}\boldsymbol{O}^{\top} = \boldsymbol{I}_n$, which should not be confused with the computational complexity $O(n)$). Since these transformations essentially just rotate the basis to define the coordinate system, they must not affect intrinsic information like data variability, signal intensity or the energy of a system. The eigenvalues are able to capture some of these inherent information, but recovering the complete general information requires computing their respective eigenvectors (for example to find the principal component, the direction of the signal or the physical state). There are more such invariants than eigenvalues. Another important set worth mentioning are the traces of the n first matrix powers $\mathrm{Tr}(\boldsymbol{A}), \mathrm{Tr}\big(\boldsymbol{A}^2\big), \ldots, \mathrm{Tr}(\boldsymbol{A}^n)$. Obtaining them uses slightly different methods than eigenvalues, but they contain the same information since each set can be inferred from the other through some basic algebraic operations.

On the basis of the matrix case, we expect that for a tensor $\mathsf{T} \in \bigotimes_{i=1}^{k} \mathbb{R}^{n_i}$, tensor quantities that are invariant under orthogonal transformations ($\mathsf{T}_{a_j^1 \ldots a_j^k} \to O^{(1)}_{a_j^1 b_j^1} \ldots O^{(k)}_{a_j^k b_j^k} \mathsf{T}_{b_j^1 \ldots b_j^k}$ for $\boldsymbol{O}^{(i)} \in \mathrm{O}(n_i) \quad \forall i \in [k]$) should capture similar intrinsic information like the intensity of the signal, and conceivably, there should be other objects related to these quantities that are able to indicate the direction of the signal. However, the concept of eigenvalue and eigenvector is ill defined in the tensor case and not practical giving that the number of eigenvalues is exponential with the dimension n (Qi (2005), Cartwright & Sturmfels (2013)) and computing them is very complicated. In contrast, we have a very convenient generalization of the traces of the power matrices for the tensors that we call trace invariants. They have been extensively studied during the last years in the context of high energy physics and many important properties have been proven (Gurau (2017)).

We first give a more formal definition of trace invariants. Let T be a tensor whose entries are $\mathsf{T}_{i_1,\ldots,i_k}$. Let's define a contraction of a pair of indices as setting them equal to each other and summing over them, as in calculating the trace of a matrix ($\boldsymbol{A}_{ij} \to \sum_{i=1}^{n} \boldsymbol{A}_{ii}$). The trace invariants of the tensor T correspond to the different way to contract pairs of indices in a product of an even number of copies of T. The degree of the trace invariants consists in the number of copies of T contracted. For example, $\sum_{i_1,i_2,i_3} \mathsf{T}_{i_1 i_2 i_3}\mathsf{T}_{i_1 i_2 i_3}$ and $\sum_{i_1,i_2,i_3} \mathsf{T}_{i_1 i_2 i_2}\mathsf{T}_{i_1 i_3 i_3}$ are trace invariants of degree 2. In the remainder of this paper, we will use the Einstein summation convention defined in the notation subsection.

A trace invariant of degree d of a tensor T of order k admits a practical graphical representation as an edge colored graph $\mathcal{G}$ obtained by following two steps: we first draw d vertices representing the d

different copies of $\mathbf{T}$. The indices of each copy is represented by k half-edges with a different color for each index position as shown in Figure 1a. Then, when two different indices are contracted in the tensor invariant, we connect their corresponding half-edges in $\mathcal{G}$. Reciprocally, to obtain the tensor invariant associated to a graph $\mathcal{G}$ with d vertices, we take d copies of $\mathbf{T}$ (one for each vertex), we associate a color for each index position, and we contract the indices of the d copies of $\mathbf{T}$ following the coloring of the edges connecting the vertices. We denote this invariant $I_{\mathcal{G}}(\mathbf{T})$. Three important examples of trace invariants are: the melon diagram (Figure 1b), the tetrahedral (1c) and the tadpole (1d). Avohou et al. (2020) provides a thorough study about the number of trace invariants for a given degree d. A very useful asset of these invariants is that we are able to compute their expectation for tensors whose components are Gaussian using simple combinatorial analysis (Gurau (2017)).

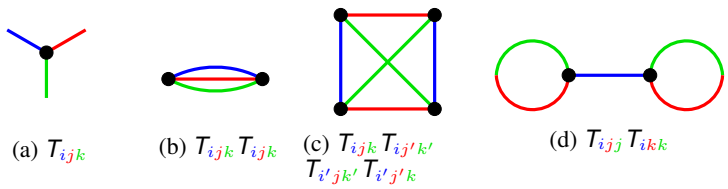

Figure 1: Example of graphs and their associated invariants

2.2 What do we use to recover the signal?

As previously mentioned in Section 2.1, an invariant should be able to detect a signal. But if our goal is to recover it, we should find mathematical objects that are able to provide a vector. To this effect, we introduce in this paper a new set of tools in the form of matrices. We denote by $\boldsymbol{M}_{\mathcal{G},e}$ the matrix obtained by cutting an edge e of a graph $\mathcal{G}$ in two half edges (see Figure 2 for an example). Indeed, this cut amounts to not summing over the two indices i_1 and i_2 associated to these two half-edges and using them to index the matrix instead. We will drop the index $\mathcal{G}, e$ of the matrix when the context is clear.

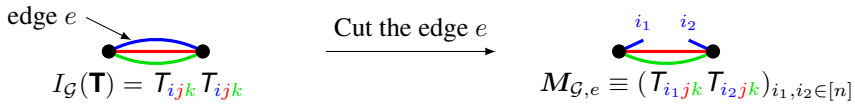

Figure 2: Obtaining a matrix by cutting the edge of a trace invariant graph $\mathcal{G}$

2.3 Phase Transition within this Framework

We can represent the tensor from which we hope to extract the signal represented graphically as:

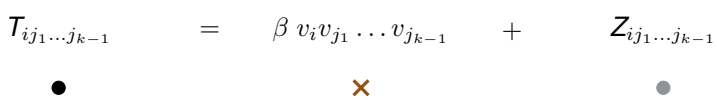

Figure 3: Graphical decomposition of the tensor $\mathbf{T}$

This decomposition leads us naturally to decompose in a similar way a tensor trace invariant $I_{\mathcal{G}}(\mathbf{T})$ into two parts, separating a first contribution $I_{\mathcal{G}}^{(N)}(\mathbf{T})$ associated to the pure noise tensor contribution and a second part $I_{\mathcal{G}}^{(S)}(\mathbf{T})$ enclosing all the other contributions, which are resulting from the addition of the signal.

$$I_{\mathcal{G}}(\mathbf{T}) = I_{\mathcal{G}}^{(N)}(\mathbf{T}) + I_{\mathcal{G}}^{(S)}(\mathbf{T}). \tag{2}$$

An identical decomposition can be carried out for the matrix. Let's consider a tensor $\mathbf{T}$, a graph $\mathcal{G}$ and its associated trace invariant $I_{\mathcal{G}}(\mathbf{T})$. Let's denote $I'_{\mathcal{G}}(\mathbf{T})$ the invariant associated to the subgraph obtained by removing from $\mathcal{G}$ the edge e and its two vertices. We can distinguish three kind of

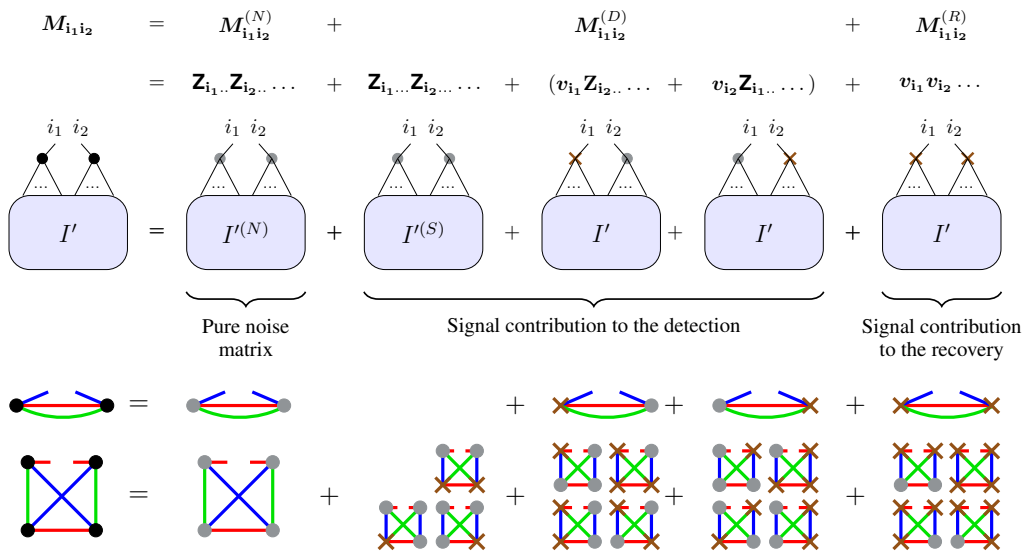

Figure 4: Decomposition of a matrix graph and the melon example

contributions to the matrix $\boldsymbol{M}_{\mathcal{G},e}$ that we denote $\boldsymbol{M}^{(N)}_{\mathcal{G},e}$, $\boldsymbol{M}^{(D)}_{\mathcal{G},e}$ and $\boldsymbol{M}^{(R)}_{\mathcal{G},e}$, illustrated in Figure 4 (where we denoted the invariant $I'_{\mathcal{G}}(\mathbf{T})$ by I' and dropped the index $\mathcal{G}, e$ for simplicity).

Lemma 1. $\mathbb{E}(\boldsymbol{M}^{(N)}) = \frac{\mathbb{E}(I^{(N)}_{\mathcal{G}})}{n}\boldsymbol{I}_n$.

Using the lemma 1, we identify three possible phases depending on which matrix operator norm is much larger than the others:

- **No detection and no recovery:** If $\left\|\boldsymbol{M}^{(N)} - \mathbb{E}(\boldsymbol{M}^{(N)})\right\|_{\text{op}} \gg \left\|\boldsymbol{M}^{(D)}\right\|_{\text{op}}, \left\|\boldsymbol{M}^{(R)}\right\|_{\text{op}}$ then no recovery and no detection is possible we can't distinguish if there is a signal. It is for example the phase for $\beta \to 0$.
- **Detection but no recovery:** If $\left\|\boldsymbol{M}^{(D)}\right\|_{\text{op}} \gg \left\|\boldsymbol{M}^{(N)} - \mathbb{E}(\boldsymbol{M}^{(N)})\right\|_{\text{op}}, \left\|\boldsymbol{M}^{(R)}\right\|_{\text{op}}$ then detection but no recovery. We can detect the presence of the signal (thanks to the highest eigenvalue) but we can't recover the signal vector since the leading eigenvector is not correlated to the signal vector.
- **Detection and recovery:** $\left\|\boldsymbol{M}^{(R)}\right\|_{\text{op}} \gg \left\|\boldsymbol{M}^{(N)} - \mathbb{E}(\boldsymbol{M}^{(N)})\right\|_{\text{op}}, \left\|\boldsymbol{M}^{(D)}\right\|_{\text{op}}$. We recover the signal vector. It is for example the phase for $\beta \to \infty$.

2.4 Algorithmic Threshold for a General Graph

We can now state the important algorithms that will be essential for this paper. It is important to keep in mind that the following claims concern the large n limit. Empirically, the approximation of large n limit seems valid for $n > 25$.

Algorithm 1: Detection algorithm associated to the graph $\mathcal{G}$ and edge e

Input: The tensor $\mathbf{T} = \beta \boldsymbol{v}^{\otimes k} + \mathbf{Z}$
Goal: Detection of $\boldsymbol{v}$
1 Calculate the scalar $\alpha = I_{\mathcal{G}}(\mathbf{T})$;
2 Compare $|\alpha - \mathbb{E}(I_{\mathcal{G}}(\mathbf{B}))|$ with the variance $\sigma(I_{\mathcal{G}}(\mathbf{B}))$ where the components of the tensor $\mathbf{B}$ follows a Gaussian random distribution.
Result: Gives the probability of the presence of a spike

The first algorithm gives a criteria for distinguishing a pure noise tensor from a tensor with a spike. Denoting $\mathbb{E}(I_{\mathcal{G}}(\mathbf{B}))$ the expectation and $\sigma(I_{\mathcal{G}}(\mathbf{B}))$ the variance of the trace invariant associated to a graph $\mathcal{G}$ for $(\mathbf{B})$), where the components of $\mathbf{B}$ are Gaussian random. The algorithm consists

simply in calculating the trace invariant of the tensor and comparing its distance from $\mathbb{E}(I_{\mathcal{G}}(\mathbf{B}))$ with $\sigma(I_{\mathcal{G}}(\mathbf{B}))$. It is straightforward to see that calculating a trace invariant (which is a scalar) like $T_{ijk}T_{ijk}$ only needs $O(1)$ memory.

Theorem 2. *Let $\mathcal{G}$ be a graph of degree d, $\exists\ \beta_{det} > 0$ so that Algorithm 1 detects the presence of a signal for $\beta \geq \beta_{det}$.*

The second algorithm is able to recover the spike in a tensor $\mathbf{T}$ through the construction of the matrix of size $n \times n$ $\boldsymbol{M}_{\mathcal{G},e}(\mathbf{T})$ associated to a given graph $\mathcal{G}$ and edge e.

Algorithm 2: Recovery algorithm associated to the graph $\mathcal{G}$ and edge e

Input: The tensor $\mathbf{T} = \beta \boldsymbol{v}_0^{\otimes k} + \mathbf{Z}$
Goal: Estimate $\boldsymbol{v}_0$
1 Calculate the matrix $\boldsymbol{M}_{\mathcal{G},e}(\mathbf{T})$;
2 Compute its top eigenvector by matrix power iteration (repeat $v_i \leftarrow M_{ij}v_j$).
Result: Obtaining an estimated vector $\boldsymbol{v}$

Theorem 3. *Let $\mathcal{G}$ be a graph of degree d, $\exists\ \beta_{rec} > 0$ so that Algorithm 2 gives an estimator $\boldsymbol{v}$ so that $\boldsymbol{v}$ is strongly correlated to $\boldsymbol{v}_0$ ($\langle \boldsymbol{v}, \boldsymbol{v}_0 \rangle > 0.9$) for $\beta \geq \beta_{rec}$.*

Since the algorithms 2 and 1 consists in algebraic operations on the tensors entries, they are very suitable for a parallel architecture. The Theorem 4 gives a lower bound to the threshold above which we can detect and recover a spike using a single graph. Interestingly, this threshold which appears naturally in our framework, matches the threshold below which there is no known algorithm that is able to recover the spike in polynomial time. We call the Gaussian variance of a graph $\mathcal{G}$, the variance of the invariant $I_{\mathcal{G}}(\mathbf{B})$ where B_{ijk} are Gaussian random.

Theorem 4. *Let $k \geq 3$. It is impossible to detect or recover the signal using a single graph below the threshold $\beta \leq n^{k/4}$ which is the minimal Gaussian variance of any graph $\mathcal{G}$.*

3 Some applications of this framework

Using these algorithms, we are now able to investigate the performance of our framework in various theoretical settings. In the first two subsections, we study the algorithms associated to two trace invariants of degree 2. They consist of the melonic diagram, which gives a very practical detection algorithm, and whose recovery algorithm is a variant of the unfolding algorithm, and the tadpole diagram whose recovery algorithm is similar to the homotopy algorithm. The third subsection goes further in terms of graph's degree and investigate the algorithms associated to the perfect one-factorization graphs (consisting in the tetrahedral when $k = 3$). The last two sections are an illustration of the versatility of this framework. We study the case the dimensions n_i of the tensor $\mathbf{T}$ ($\mathbf{T} \in \bigotimes_{i=1}^{k} \mathbb{R}^{n_i}$) are not necessarily equal, which is important for practical applications where the dimensions are naturally asymmetric. Our methods allows us to derive a new algorithmic threshold for this case. It also shows the closeness of the Tensor PCA and Tensor decomposition problems by handling the recovery of many orthogonal spikes at the same threshold of a single spike: $n^{k/4}$.

3.1 The melon graph similar to Tensor unfolding

Let's consider the invariant $T_{i_1 \dots i_n} T_{i_1 \dots i_n}$ (illustrated by the graph in Figure 1b when $k = 3$). Its recovery algorithm (with the matrix obtained by cutting any of the edges) is similar to the tensor unfolding method presented in Richard & Montanari (2014). The difference is that the melonic algorithm uses only a matrix $n \times n$ instead of a matrix $n^{k/2} \times n^{k/2}$ for the tensor unfolding. However, the main contribution of this framework for this graph is that it allows the detection in a linear time (n^k operations for a input (tensor) of size n^3) in a constant memory space (it just calculates a scalar). This provides it a potential usefulness as a first step for detecting the signal before deciding to use more computationally costly methods to recover it. Also, to the best of our knowledge, this framework is the first to theoretically prove a conjuncture that the unfolding algorithm works also for the symmetric case.

Theorem 5. *The algorithms 1 and 2 work for the melon graph with $\beta_{det} = \beta_{rec} = O(n^{k/4})$ in linear time and respectively $O(n^2)$ and $O(1)$ memory requirement.*

3.2 THE TADPOLE GRAPH

Figure 1d has a special characteristic: we can obtain two disconnected parts by cutting only one line. Therefore, the matrix obtained by cutting that edge is of rank one (in the form of $\boldsymbol{v}\boldsymbol{v}^T$). Thus, the vector $\boldsymbol{v}$ has a weak correlation with the signal $\boldsymbol{v}_0$, which allow the tensor power iteration ($v_i \leftarrow \mathsf{T}_{ijk} v_j v_k$) to empirically recover it (formal proofs require to consider some more sophisticated variants of power itration like in Anandkumar et al. (2017) and Biroli et al. (2020)). This algorithm is a variant of the already existent homotopy algorithm.

Theorem 6. *The tadpole graph allows to recover the signal vector for $k \geq 3$ and $\beta = O(n^{k/4})$ by using local algorithms to enhance the signal contribution of the vector T_{ijj}.*

3.3 TENSOR INVARIANT BASED ON THE PERFECT ONE-FACTORIZATION GRAPHS

The next graph we investigate is of degree strictly superior to two. The perfect one-factorization graph (see Appendix C) has nice combinatorial properties which make it relevant as an example of non trivial graph that we investigate in order to evaluate the richness of the framework. Moreover, these properties also simplify the proofs for its detection and recovery theorems. Thus, the standard methods involved in the demonstrations of these theorems are instructive for the study of more general graphs. For $k = 3$, it is the tetrahedral graph, which shows very interesting empirical results.

Theorem 7. *The algorithm associated to a perfect one-factorization graph is able to recover the signal vector for $\beta = O(n^{k/4})$.*

3.4 HANDLING A SPIKE WITH DIFFERENT DIMENSIONS

We consider the more general case where the tensor $\mathbf{T}$ has axes of different dimensions n_i ($\mathbf{T} \in \bigotimes_{i=1}^k \mathbb{R}^{n_i}$). We can assume without any loss of generality that $n_1 \geq n_2 \geq \cdots \geq n_k$.

$$\mathbf{T} = \beta \boldsymbol{v}_1 \otimes \cdots \otimes \boldsymbol{v}_k + \mathbf{Z} \quad \text{where} \quad \boldsymbol{v}_i \in \mathbb{R}^{n_i}, \quad n_i \in \mathbb{N}. \tag{3}$$

Our framework naturally handles this case and allow us to derive a new algorithmic threshold. It is, to the best of our knowledge, the first generalization of the threshold $\beta = n^{k/4}$ derived in Richard & Montanari (2014) when $n_i = n \; \forall i \in [k]$.

Theorem 8. *Using the melon graph, the threshold for $\boldsymbol{v}_1$ is given by $\max\left((\prod_{i=1}^k n_i)^{1/4}, n_1^{1/2}\right)$ while the thresholds for $\boldsymbol{v}_j,\ j \geq 2$ are equal to $(\prod_{i=1}^k n_i)^{1/4}$.*

This result coincides with the previously known threshold when $n_i = n$. Also the threshold $\max\left((\prod_{i=1}^k n_i)^{1/4}, n_1^{1/2}\right)$ for $\boldsymbol{v}_1$ is not surprising. Indeed, if $n_2 = \cdots = n_k = 1$, the tensor can be seen as a vector of dimension n_1. And since the expectation of the norm of a random gaussian vector is $n_1^{1/2}$ we would need $\beta > n_1^{1/2}$ and not $\beta > n_1^{1/4}$ to be able to detect the signal vector.

3.5 HANDLING MULTIPLE ORTHOGONAL SPIKES

We consider a symmetric tensor with multiple orthogonal spikes.

$$\mathbf{T} = \sum_{i=1}^{p} \beta_i \boldsymbol{v}_i^{\otimes k} + \mathbf{Z} \quad \text{where} \quad \langle \boldsymbol{v}_i, \boldsymbol{v}_j \rangle = 0 \quad \forall i \neq j. \tag{4}$$

Theorem 9. *If we have a number of spikes p that is constant in respect to n, we can recover the p spikes by an alternating the use of melonic diagram, power iteration and deflation.*

We first use the melonic diagram to obtain a vector correlated with the signal vectors, then we follow by power iteration to obtain a normalized vector $\boldsymbol{v}$ highly correlated to one of the spikes and then deflation which consists in replacing the tensor $\mathbf{T}$ by $\mathbf{T} - \alpha \boldsymbol{v}^{\otimes 3}$ where $\alpha = \mathbf{T}.\boldsymbol{v}^{\otimes 3}$. The experimental results suggest that it works not only for small values of p but also for a number of spikes up to n.

4 NUMERICAL EXPERIMENTS

In this section we will investigate the empirical results of the previously mentioned applications in order to see if they match with our theoretical results. We restrict to the dimension $k = 3$ for simplicity. More details about the experiments settings could be found in the Appendix D.

4.1 DETECTION AND COMPARISON OF RECOVERY METHODS

Our detection algorithm, based on the melon graph, uses the fact that the distributions of $\mathbf{T}_{ijk}\mathbf{T}_{ijk}$ for $\mathbf{T} = \mathbf{Z}$ and for $\mathbf{T} = \mathbf{Z} + \beta \boldsymbol{v}^{\otimes 3}$ become distinct when β is large enough, where the components of $\mathbf{Z}$ follows a Gaussian random distribution and $\boldsymbol{v}$ an unitary vector. This distinction is easily visible, for $n = 100$ and $\beta = 100$ in Figure 5a where we plotted the histograms of the melonic invariant (in blue without signal and in orange with signal) for 500 independent instances of Gaussian random tensors $\mathbf{Z}$. Thus, to measure the accuracy of the detection of the signal, we use the quantity: 1 - cardinal of the Intersection over the cardinal of the Union (1-IoU). Figure 5b suggests that a high probability detection requires $\beta \geq 3n^{3/4}$.

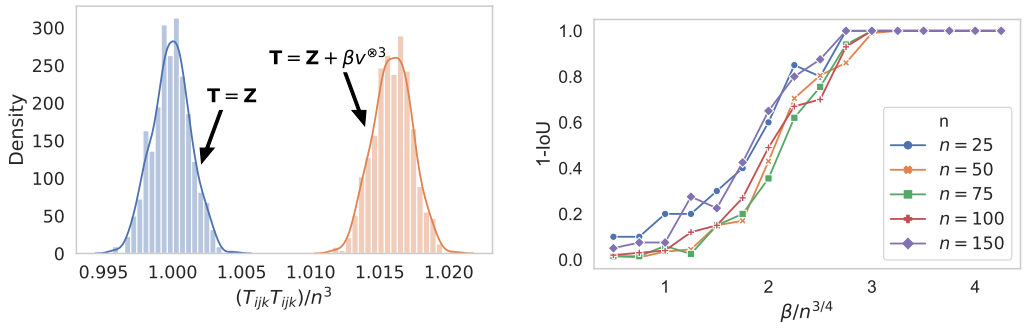

(a) Distribution of the melon invariant without (blue) and with (orange) signal.

(b) Detection threshold for different n.

Figure 5: Detection using the melonic graph.

For the recovery algorithm, we focus in the symmetric case (the most studied case and the most consistent with a symmetric spike) and, as in Richard & Montanari (2014), for every algorithm we use two variants: the simple algorithm outputting $\boldsymbol{v}$ and an algorithm where we apply 100 power iterations on $\boldsymbol{v}$: $v_i \leftarrow T_{ijk}v_jv_k$, distinguishable by a prefix "p-". In Figure 6, we run 200 experiments for each value of β and plot the 95% confidence interval of the correlation of the vector recovered with the signal vector. We will compare our method (tetrahedral) to two type of results:

- Other algorithmic methods: the melonic (tensor unfolding) and the homotopy. To the best of our knowledge, they give the state of art respectively for the symmetric and asymmetric tensor (Biroli et al. (2020)). Other methods exist but are either too computationally expensive (sum of squares) or are variants of these algorithms.
- Information-theoretical results: In (Richard & Montanari (2014)), it was proven that computing the global minimum $\boldsymbol{v}$ of the function $\boldsymbol{v} \mapsto T_{ijk}v_iv_jv_k$ recovers the signal vector $\boldsymbol{v}_0$ above a theoretical threshold $\beta_{\text{th}} = 2.87\sqrt{n}$ but with exponential time, and that no other approach can do significantly better than that. Thus, to assess the performance of the tetrahedral, we plot in red dashed line denoted "perf" the deep minimum that is closest to $\boldsymbol{v}_0$, by using gradient method with an initialization in $\boldsymbol{v}_0$. Interestingly, we note that not only the tetrahedral is able perform better than other methods, but is able as well to recover the spike at nearly the theoretical threshold even at $n \sim 100$.

4.2 A SPIKE WITH DIFFERENT DIMENSIONS AND MULTIPLE SPIKES

We aim to recover the three vectors $\boldsymbol{v}_1, \boldsymbol{v}_2$ and $\boldsymbol{v}_3$ of the spike $\boldsymbol{v}_1 \otimes \boldsymbol{v}_2 \otimes \boldsymbol{v}_3$. We repeat 100 times each instance consisting in choosing randomly $\boldsymbol{v}_1, \boldsymbol{v}_2$ and $\boldsymbol{v}_3$ and the Gaussian random tensor $\mathbf{Z}$ and

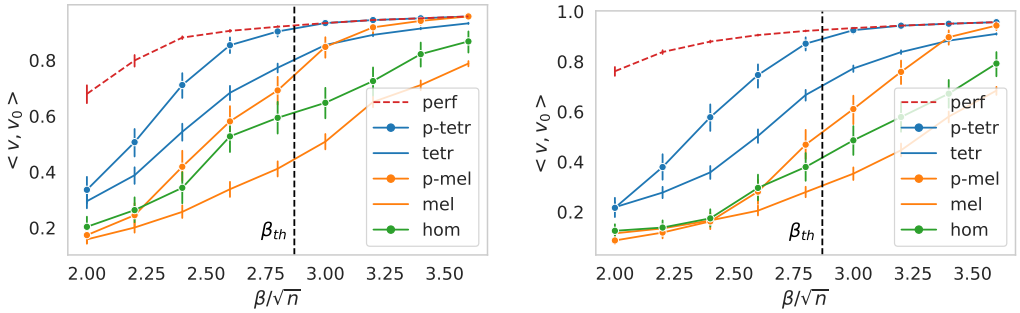

Figure 6: Comparison of different methods for symmetric recovery. Left: n=100, right: n=150.

we plot the correlation of the signal vectors with the vectors recovered from $\mathbf{Z} + \beta \boldsymbol{v}_1 \otimes \boldsymbol{v}_2 \otimes \boldsymbol{v}_3$ using the tetrahedral. We see in the Figure 7a that the threshold $(n_1 n_2 n_3)^{1/4}$ for the three vectors matches perfectly with the experiences when $n_3 < n_1.n_2$. We also see that when $n_3 > n_1.n_2$ the recovery of v_3 (in green and with the diamond and square markers) have a different asymptotic behavior than v_1 and v_2 (it becomes $n_3^{1/2}$ since $n_3^{1/2} \geq (n_1 n_2 n_3)^{1/4}$), corresponding to what our theoretical study predicted. In 7b, we plot the correlation between the 100 orthogonal spikes $\boldsymbol{v}_i$ and their corresponding recovered vectors $\boldsymbol{w}_i$ when β_i are all equal for $n = 100$. The results suggest that the threshold to recover multiple spikes is similar to the threshold of only one spike.

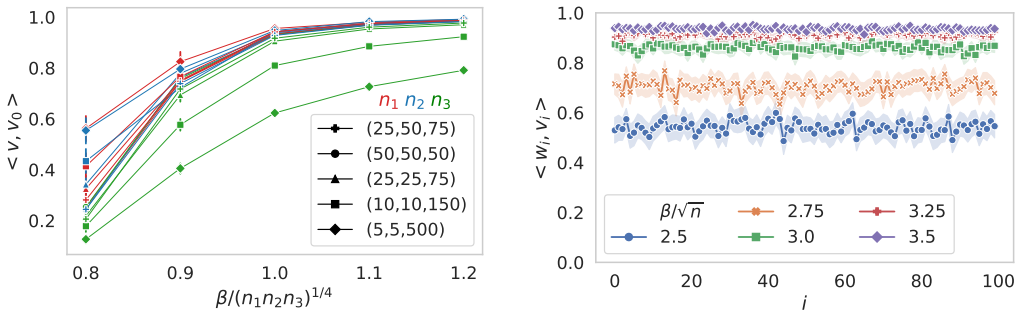

(a) Recovery of a spike with different dimensions.

(b) Recovery of 100 orthogonal spikes for different β.

Figure 7: Signal with different dimensions (left). Multiple orthogonal spikes for n=100 (right).

5 Conclusion

In this paper we introduced a novel framework for the tensor PCA based on trace invariants. Within this framework, we provide different algorithms to detect a signal vector or recover it. These algorithms use tensor contractions that has a high potential of parallelization and computing optimization. We illustrate the practical pertinence of our framework by presenting some examples of algorithms and prove their ability to detect and recover a signal vector linearly in time for β above the optimal algorithmic threshold. Note that, one of the proposed detection algorithms requires only $O(1)$ memory requirement which could be advantageous in some applications. Our experimental results show that the tetrahedral graph performs better than the the state of the art in the symmetric case. Moreover, we also show that two well known algorithms (Homotopy and Tensor Unfolding) can be mapped to our framework and result to simpler graph (e.g. the melonic graph). Interestingly, our framework is also able to extend the theoretical and practical study of tensor PCA to new and less restrictive situations like data where the dimensions of the axes are different or a sum of orthogonal spikes. Important directions of future research is to explore the potential of more general graphs and to try to apply these new methods to real data.

REFERENCES

Anima Anandkumar, Dean P Foster, Daniel Hsu, Sham M Kakade, and Yi-Kai Liu. A spectral algorithm for latent dirichlet allocation. *Algorithmica*, 72(1):193–214, 2015.

Anima Anandkumar, Yuan Deng, Rong Ge, and Hossein Mobahi. Homotopy analysis for tensor pca. In *Conference on Learning Theory*, pp. 79–104. PMLR, 2017.

Animashree Anandkumar, Rong Ge, Daniel Hsu, Sham M Kakade, and Matus Telgarsky. Tensor decompositions for learning latent variable models. *Journal of Machine Learning Research*, 15: 2773–2832, 2014.

Gerard Ben Arous, Reza Gheissari, Aukosh Jagannath, et al. Algorithmic thresholds for tensor pca. *Annals of Probability*, 48(4):2052–2087, 2020.

Remi C. Avohou, Joseph Ben Geloun, and Nicolas Dub. On the counting of $O(N)$ tensor invariants. *Adv. Theor. Math. Phys.*, 24(4):821–878, 2020. doi: 10.4310/ATMP.2020.v24.n4.a1.

Kamyar Azizzadenesheli, Alessandro Lazaric, and Animashree Anandkumar. Reinforcement learning of pomdps using spectral methods. In *29th Annual Conference on Learning Theory*, volume 49 of *Proceedings of Machine Learning Research, publisher = PMLR*, pp. 193–256, 2016.

Jinho Baik, Gérard Ben Arous, Sandrine Péché, et al. Phase transition of the largest eigenvalue for nonnull complex sample covariance matrices. *The Annals of Probability*, 33(5):1643–1697, 2005.

Giulio Biroli, Chiara Cammarota, and Federico Ricci-Tersenghi. How to iron out rough landscapes and get optimal performances: averaged gradient descent and its application to tensor PCA. *Journal of Physics A Mathematical General*, 53(17):174003, May 2020.

Giulio Biroli, Chiara Cammarota, and Federico Ricci-Tersenghi. How to iron out rough landscapes and get optimal performances: averaged gradient descent and its application to tensor pca. *Journal of Physics A: Mathematical and Theoretical*, 53(17):174003, 2020.

Dustin Cartwright and Bernd Sturmfels. The number of eigenvalues of a tensor. *Linear algebra and its applications*, 438(2):942–952, 2013.

Rishabh Dudeja and Daniel Hsu. Statistical Query Lower Bounds for Tensor PCA. *arXiv e-prints*, art. arXiv:2008.04101, August 2020.

Oleg Evnin. Melonic dominance and the largest eigenvalue of a large random tensor. *arXiv preprint arXiv:2003.11220*, 2020.

Frank Ferrari, Vincent Rivasseau, and Guillaume Valette. A New Large N Expansion for General Matrix–Tensor Models. *Commun. Math. Phys.*, 370(2):403–448, 2019.

Lianli Gao, Jingkuan Song, Xingyi Liu, Junming Shao, Jiajun Liu, and Jie Shao. Learning in high-dimensional multimedia data: the state of the art. *Multimedia Systems*, 23(3):303–313, 2017.

Izrail Gelfand. Normierte ringe. 9(1):3–24, 1941.

R. Gurau. *Random Tensors*. Oxford University Press, 2017.

Razvan Gurau. Universality for Random Tensors. *Ann. Inst. H. Poincare Probab. Statist.*, 50(4): 1474–1525, 2014.

Razvan Gurau. On the generalization of the wigner semicircle law to real symmetric tensors. *arXiv preprint arXiv:2004.02660*, 2020.

Matthew B. Hastings. Classical and Quantum Algorithms for Tensor Principal Component Analysis. *Quantum*, 4:237, February 2020.

Samuel B. Hopkins, Jonathan Shi, and David Steurer. Tensor principal component analysis via sum-of-squares proofs. *CoRR*, abs/1507.03269, 2015.

Jianyu Huang, Devin A Matthews, and Robert A van de Geijn. Strassen's algorithm for tensor contraction. *SIAM Journal on Scientific Computing*, 40(3):C305–C326, 2018.

Majid Janzamin, Hanie Sedghi, and Anima Anandkumar. Beating the perils of non-convexity: Guaranteed training of neural networks using tensor methods. *arXiv preprint arXiv:1506.08473*, 2015.

I. T. Jolliffe and Jorge Cadima. Principal component analysis: a review and recent developments. *Philosophical Transactions of the Royal Society A: Mathematical, Physical and Engineering Sciences*, 374, 2016.

Jinsung Kim, Aravind Sukumaran-Rajam, Changwan Hong, Ajay Panyala, Rohit Kumar Srivastava, Sriram Krishnamoorthy, and Ponnuswamy Sadayappan. Optimizing tensor contractions in ccsd (t) for efficient execution on gpus. In *Proceedings of the 2018 International Conference on Supercomputing*, pp. 96–106, 2018.

T. Kolda and B. Bader. Tensor decompositions and applications. *SIAM Rev.*, 51:455–500, 2009.

Wenjing Ma, Sriram Krishnamoorthy, Oreste Villa, Karol Kowalski, and Gagan Agrawal. Optimizing tensor contraction expressions for hybrid cpu-gpu execution. *Cluster computing*, 16(1): 131–155, 2013.

Devin A Matthews. High-performance tensor contraction without transposition. *SIAM Journal on Scientific Computing*, 40(1):C1–C24, 2018.

Liqun Qi. Eigenvalues of a real supersymmetric tensor. *Journal of Symbolic Computation*, 40(6): 1302 – 1324, 2005.

Emile Richard and Andrea Montanari. A statistical model for tensor pca. In *Advances in Neural Information Processing Systems*, pp. 2897–2905, 2014.

Valentina Ros, Gerard Ben Arous, Giulio Biroli, and Chiara Cammarota. Complex energy landscapes in spiked-tensor and simple glassy models: Ruggedness, arrangements of local minima, and phase transitions. *Physical Review X*, 9(1):011003, 2019.

Sheldon Ross. *A first course in probability*. Pearson, 2014.

Mohamed El Amine Seddik, Mohamed Tamaazousti, and Romain Couillet. A kernel random matrix-based approach for sparse pca. In *International Conference on Learning Representations (ICLR)*, 2019.

Nicholas D Sidiropoulos, Lieven De Lathauwer, Xiao Fu, Kejun Huang, Evangelos E Papalexakis, and Christos Faloutsos. Tensor decomposition for signal processing and machine learning. *IEEE Transactions on Signal Processing*, 65(13):3551–3582, 2017.

G. W. Stewart and Ji guang Sun. *Matrix Perturbation Theory*. Academic Press, 1990.

Taiji Suzuki. Adaptivity of deep reLU network for learning in besov and mixed smooth besov spaces: optimal rate and curse of dimensionality. In *International Conference on Learning Representations*, 2019.

David G. Wagner. On the perfect one—factorization conjecture. *Discrete Mathematics*, 104(2):211 – 215, 1992.

Per-Åke Wedin. Perturbation bounds in connection with singular value decomposition. *BIT Numerical Mathematics*, 12(1):99–111, 1972.

Alexander S Wein, Ahmed El Alaoui, and Cristopher Moore. The kikuchi hierarchy and tensor pca. In *Annual Symposium on Foundations of Computer Science (FOCS)*, pp. 1446–1468. IEEE, 2019.

A USEFUL THEOREMS

The following theorems will be useful for the demonstrations of the proposed theorems.

- **Wedin perturbation** (Wedin (1972)): Let $\boldsymbol{M} = \beta \boldsymbol{v}_0 \boldsymbol{v}_0^\top + \boldsymbol{N}$ a square matrix with $\|\boldsymbol{v}_0\| = 1$. Let $\boldsymbol{v}$ denote the eigenvector with the largest eigenvalue of $\boldsymbol{M}$. If $\beta > 2\|\boldsymbol{N}\|_{\text{op}}$ then:

$$1 - \langle \boldsymbol{v}, \boldsymbol{v}_0 \rangle \leq \frac{8\|\boldsymbol{N}\|_{\text{op}}}{\beta^2}. \tag{5}$$

- **Chebyshev inequality** (Ross (2014)): Let X be a random variable with finite expected value μ and finite non-zero variance σ^2. Then for any real number $C > 0$,

$$\Pr(|X - \mu| \geq C\sigma) \leq \frac{1}{C^2}. \tag{6}$$

  where Pr denotes the probability.

- **Gelfand's Formula** (Gelfand (1941)): For any matrix norm $\|.\|$, we have:

$$\rho(\boldsymbol{A}) = \lim_{s \to \infty} \|\boldsymbol{A}^s\|^{\frac{1}{s}}. \tag{7}$$

  where $\rho(\boldsymbol{A})$ is the spectral radius of $\boldsymbol{A}$: the largest absolute value of its eigenvalues.
  In particular, if $\boldsymbol{A}$ is a real matrix, we can choose the Frobenius norm:

$$\|\boldsymbol{A}\|_{\text{F}} = \sqrt{\text{trace}(\boldsymbol{A}^\top \boldsymbol{A})}. \tag{8}$$

B GAUSSIAN MEASURE

We will follow a similar approach to the one in Gurau (2017) to compute the expectations of trace invariants of a random tensor $\mathbf{T}$ whose components are normally distributed.

Let's consider a graph $\mathcal{G}$ of order d associated to a trace invariant $I_{\mathcal{G}}(\mathbf{T})$ where $\mathbf{T}$ is a tensor of order k. Since the trace invariant is a contraction of pairs of indices of d copies of $\mathbf{T}$, we denote the c-th index of the i-th copy of $\mathbf{T}$ by ${a_i}^c$ and the set of the d indices of the i-th copy by ${a_j}^{\mathcal{D}}$. By the definition of the Gaussian measure we have the equation:

$$\mathbb{E}(\text{Tr}_{\mathcal{G}}(\mathbf{T})) = \sum_a \delta_{aa}^{\mathcal{G}} \sum_{\tau \in \mathfrak{S}(k)} \prod_{j=1}^{k} \delta_{{a_j}^{\mathcal{D}} {a_j}_{\tau(j)}^{\mathcal{D}}}, \tag{9}$$

where $\mathfrak{S}(k)$ is the symmetric group (the group of all permutations of a set made of n elements, where we define a permutation of a set by an arrangement of its elements in a linear order. For example the permutations of $\{1, 2, 3\}$ are $(1, 2, 3), (1, 3, 2), (2, 1, 3), (2, 3, 1), (3, 1, 2), (3, 2, 1)$.).

$\sum_a$ indicates a sum over all the indices involved in the computation of the trace invariant, illustrated by a half-edge in the graph (we have $k \times d$ indices in total: k indices for each one of the d copies of $\mathbf{T}$ of the trace invariant expression). $\delta_{aa}^{\mathcal{G}}$ indicates that contracted indices (illustrated by being two ends of the same edge) of the tensors have to be equal. The term $\delta_{{a_j}^{\mathcal{D}} {a_j}_{\tau(j)}^{\mathcal{D}}}$ indicates that we set equal the c-th indices of the copy j and $\tau(j)$ of $\mathbf{T}$ for $c \in \{1, \ldots, d\}$

In order to have a clearer representation of the expression in equation 9, in particular the sum over the symmetric group, we introduce the concept of covering graph used in Gurau (2014): a covering graph of $\mathcal{G}$ consists in adding $d/2$ new edges of color 0 (also called propagators) relying pairwise the vertices of $\mathcal{G}$ (Figure 8 for an example). We use the covering graphs to illustrate the permutations $\tau \in \mathfrak{S}(k)$. Then, an edge of color 0 between two vertices i and j will identify all the indices of the i-th and j-th copies of $\mathbf{T}$. Thus, it will be equivalent to the term $\delta_{{a_j}^{\mathcal{D}} {a_j}_{\tau(j)}^{\mathcal{D}}}$. Using the covering graph, we will be able to rewrite equation 9.

For example, in the case where the edges could have only one color, we have the formula:

$$\mathbb{E}(\mathrm{Tr}_{\mathcal{G}}(\mathbf{T})) = \sum_{\mathcal{G}',\mathcal{G}'\backslash\mathcal{E}^0(\mathcal{G}')=\mathcal{G}} \sum_{aa} \left(\prod_{c=1}^{3} \prod_{e^c=(v_j,v_k)\in\mathcal{E}^c(\mathcal{G})} \delta_{a_{j^c},a_{k^c}} \right) \left(\prod_{e^0=(v_p,v_q)\in\mathcal{E}^0(\mathcal{G})} \delta_{a_{p^1},a_{q^1}} \delta_{a_{p^2},a_{q^2}} \delta_{a_{p^3},a_{q^3}} \right), \tag{10}$$

Where we denote $\mathcal{E}^c(\mathcal{G})$ the set of edges of color c of $\mathcal{G}$. Thus $\{\mathcal{G}', \mathcal{G}'\backslash\mathcal{E}^0(\mathcal{G}') = \mathcal{G}\}$ denotes the graphs which restrict to the graph $\mathcal{G}$ when we remove their edges of color 0, which are by the definition the covering graphs.

Let $c_1, c_2 \in \{0, \dots, d\}$ be two different colors of edges. We denote $F^{c_1,c_2}(\mathcal{G})$ the number of closed cycles (that we also call face) of 2 colors of $\mathcal{G}$. More explicitly, it consists of the number of connected subgraphs left when we keep in $\mathcal{G}$ only the edges of colors c_1, c_2 (see Figure 9 for an illustration). We denote $F(\mathcal{G}) \equiv \sum_{c_1\neq c_2\in\{1,\dots,d\}} F^{c_1,c_2}(\mathcal{G})$.

Then, with a little work (see Gurau (2014) for a proof), we obtain :

$$\mathbb{E}(\mathrm{Tr}_{\mathcal{G}}(\mathbf{T})) = \sum_{\mathcal{G}',\mathcal{G}'\backslash\mathcal{E}^0(\mathcal{G}')=\mathcal{G}} n^{F(\mathcal{G}')-F(\mathcal{G})} = \sum_{\mathcal{G}',\mathcal{G}'\backslash\mathcal{E}^0(\mathcal{G}')=\mathcal{G}} n^{\sum_c F^{0,c}(\mathcal{G}')}. \tag{11}$$

This will be the expression we will use to calculate the expectations of our graphs if each edges has only one color.

Example: Let's calculate the expectation of the tetrahedral graph $\mathcal{B}$:

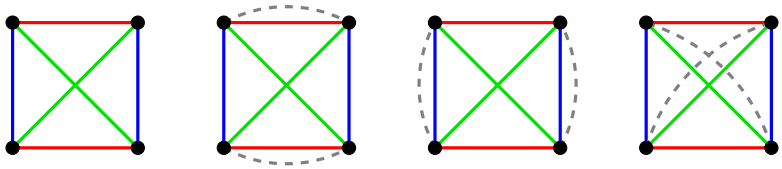

Figure 8: Tetrahedral and its covering graph

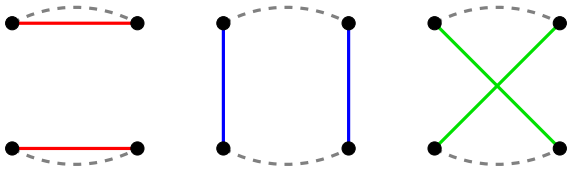

Figure 9: The faces of the first covering graph

The first step is to find all the covering graphs of the tetrahedral (drawn in Figure 8). Then, for each of the three covering graphs, and for each color c we count the number of faces associated to the colors $(0, c)$. We drawn in Figure 9 the faces for the different colors for the first graph. For every covering graph, there is one color having two faces (the red for the first covering graph) and two colors having only one face. Hence the expectation of the tetrahedral graph is given by $3n^4$:

$$\mathbb{E}(\mathrm{Tr}_{\mathcal{G}}(\mathbf{T})) = \sum_{\mathcal{G}',\mathcal{G}'\backslash\mathcal{E}^0(\mathcal{G}')=\mathcal{G}} n^{\sum_c F^{0,c}(\mathcal{G}')} = n^{2+1+1} + n^{1+2+1} + n^{1+1+2} = 3n^4. \tag{12}$$

B.1 THE CASE OF EDGES OF MIXED COLOR

For a general trace invariant, an edge can have two half edges of different colors. The propagators (edges of color 0) still identify all the indices of their two end vertices. So we adapt the steps in

Gurau (2014) to obtain the equation 13 for this new situation. More precisely, the cycles that we will count in a covering graph $\mathcal{G}'$ of $\mathcal{G}$ are built by beginning from a half-edge of $\mathcal{G}$ then alternating until they go back to the starting half-edge by:

- going from a half-edge of $\mathcal{G}$ of color $c_1 \neq 0$ to its associated half edge of color $c2$.
- going through the propagator to the half-edge of color c_2 connected to the other end of the propagator.

$$\mathbb{E}(\mathrm{Tr}_{\mathcal{G}}(\mathbf{T})) = \sum_{\mathcal{G}', \mathcal{G}' \setminus \mathcal{E}^0(\mathcal{G}') = \mathcal{G}} n^{\text{mixed cycles}} \tag{13}$$

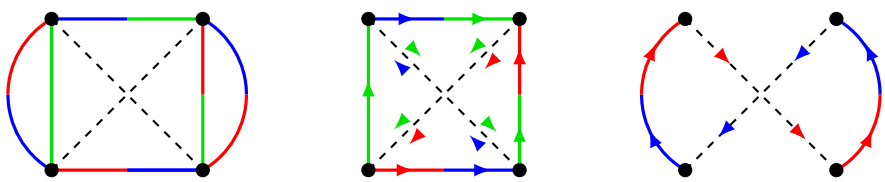

Figure 10: A mixed graph and its two cycles

B.2 THE CASE OF A GRAPH WITH AN OPEN EDGE

We encounter this case when we want to study the statistics of a matrix built out of a trace invariant graph. Indeed cutting an edge of color c removes the contraction of two indices and leaves them free as variables i_1 and i_2. Then in the formula $\left(\prod_{c=1}^{3} \prod_{e^c=(v_j,v_k)\in\mathcal{E}^c(\mathcal{G})} \delta_{a_j^c,a_k^c}\right)$ we replace $\delta_{a_j^c,a_k^c}$ by $\delta_{a_j^c,i_1}\delta_{i_2,a_k^c}$ with i_1 and i_2 fixed. Thus if a face of color $0, c$ contains only one of the two vertices of the edge (if the graph is connected, this only happens when we calculate the variance), its contribution is equal to one. If it contains the two vertices, it is equal to one if $i_1 = i_2$ and zero otherwise.

B.3 THE CASE OF A GRAPH WITH A MIX OF SPIKES AND RANDOM TENSORS

We encounter this case when we want to calculate the contribution of the signal to an invariant, which lead us to replace a vertex by the tensorial product of our signal vector. Since we are interested by an expectation, and knowing that the gaussian distribution is invariant by rotation, we may as well take the signal vector as the unit vector $(1, 0, \ldots, 0)$. Then in the formula $\left(\prod_{c=1}^{3} \prod_{e^c=(v_j,v_k)\in\mathcal{E}^c(\mathcal{G})} \delta_{a_j^c,a_k^c}\right)$ we replace $\delta_{a_j^c,a_k^c}$ by $\delta_{a_j^c,0}$ and we restrict the propagators to the tensors vertices. First, we notice that if there is an odd number of spikes, the expectation will be equal to zero. Furthermore, there is no free sum if the index identified in a cycle ends up with a contraction with a spike. Its contribution is equal to one.

C THE PERFECT ONE-FACTORIZATION GRAPH

In the mathematical field of graph theory, a graph $\mathcal{G}$ is said to be one-factorizable (Wagner (1992)) if:

- It is k-regular, which means that each vertex is incident to exactly k edges.
- Its edges can be colored in k colors such that no two incident edges have the same color.

A perfect one-factorization of $\mathcal{G}$ happens if, for every two colors c_1 and c_2 of the k colors, restricting $\mathcal{G}$ to the edges of color c_1 and c_2 leads to a single connected cycle, in other words the number of the faces associated to the colors c_1 and c_2 is always equal to one, $F^{c_1,c_2}(\mathcal{G}) = 1 \ \forall c_1, c_2$. We can see in Figure 11 that restricting to the red and green colors, or the red and blue colors, leads to a single connected cycle.

It is conjectured (Wagner (1992)) that they exist for all n but, until now, they were proven only for prime numbers and up to 56. We use this particular set of graphs because of its combinatorial simplicity. The perfect one-factorization graphs have already been studied in the context of random tensors in Ferrari et al. (2019).

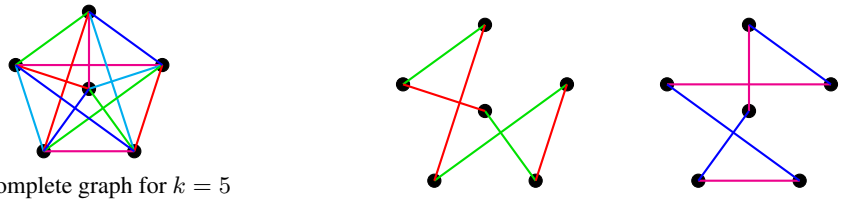

(a) Complete graph for $k = 5$

Figure 11: Complete graph for $k = 5$ and some two colors restriction

D DETAILS ON THE EXPERIMENTS

D.1 DETECTION

D.1.1 THE SETTINGS

For each of the detection figures, we repeat 500 independent instances of the following experiment:

- We generate randomly the n components of the signal vector $\boldsymbol{v}_0$ and then normalize $\boldsymbol{v}_0$.
- We generate randomly the n^3 components of the random tensor $\mathbf{Z}$. If we are in the symmetric case, we symmetrize it with the same normalization than Richard & Montanari (2014)):

$$Z_{ijk} = (Z_{ijk} + Z_{ikj} + Z_{jik} + Z_{jki} + Z_{kij} + Z_{kji})/\sqrt{12}$$

- We compute the melonic trace invariant $\mathbf{Z}_{ijk}\mathbf{Z}_{ijk}$ using the numpy method tensordot in Python.
- We compute the tensor $\mathbf{T} = \mathbf{Z} + \beta \boldsymbol{v}^{\otimes k}$
- We compute the melonic trace invariant $\mathbf{T}_{ijk}\mathbf{T}_{ijk}$ using the numpy method tensordot in Python.

Then in Figure 5a, we plot in blue the distribution of $\mathbf{Z}_{ijk}\mathbf{Z}_{ijk}$ and in orange the distribution of $\mathbf{T}_{ijk}\mathbf{T}_{ijk}$ where $\mathbf{T} = \mathbf{Z} + \beta \boldsymbol{v}^{\otimes k}$. This provides an empirical proof that the distribution of $\mathbf{T}_{ijk}\mathbf{T}_{ijk}$ is far enough from the one of $\mathbf{Z}_{ijk}\mathbf{Z}_{ijk}$ to distinguish a tensor with a signal from a Gaussian random tensor.

In Figure 5b, we plot the quantity ($1-$ cardinal of intersection of the two distributions over the cardinal of the union of the two distributions) for different n. We see that the detection, which is related to the ability to distinguish the two distributions as illustrated in Figure 5a, agrees with the threshold found theoretically $O(n^3/4)$.

D.2 RECOVERY

D.2.1 THE SETTINGS

For each of the recovery figures, we repeated 200 times the experiment in order to plot the average correlation between the vector returned by the algorithm $\boldsymbol{v}$ and the signal vector $\boldsymbol{v}_0$ and the error bars (corresponding to a 95% interval confidence).

Each experiment is an independent instance consisting in the following steps:

- We generate randomly the n components of the signal vector $\boldsymbol{v}_0$ and then normalize it.
- We generate randomly the n^3 components of the random tensor $\mathbf{Z}$. If we are in the symmetric case, we symmetrize it with the same normalization than Richard & Montanari (2014)):

$$Z_{ijk} = (Z_{ijk} + Z_{ikj} + Z_{jik} + Z_{jki} + Z_{kij} + Z_{kji})/\sqrt{12}$$

- We compute the tensor $\mathbf{T} = \mathbf{Z} + \beta \boldsymbol{v}_0^{\otimes k}$
- We compute our matrix associated to the invariant $\boldsymbol{M}$ constructed from $\mathbf{T}$ using the numpy method tensordot in Python.
- We compute its leading eigenvector $\boldsymbol{v}$
- We plot the correlation between the vector resulted from the algorithm $\boldsymbol{v}$ and the signal vector we aim to recover $\boldsymbol{v}_0$ (namely the scalar product $< \boldsymbol{v}, \boldsymbol{v}_0 >$).

D.2.2 ASYMMETRIC TENSOR WITH A SYMMETRIC SPIKE

We see that in the asymmetric case that the homotopy method, represented on our framework by the tadpole graph, performs the best. It is interesting to note that the graph that performs the best is different depending on the symmetry of the data and the symmetry of the signal.

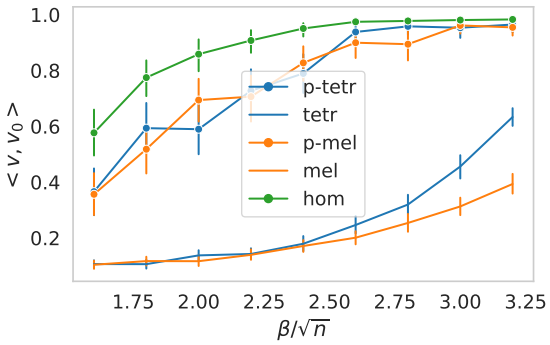

Figure 12: Recovery of $\boldsymbol{v}_3$ where $n_3 > n_1 n_2$

D.2.3 THE NUMBER OF ITERATIONS OF POWER ITERATION FOR EACH METHOD

In the symmetric case, we plot the number of iterations needed for the power iteration method to converge with an initialization given by the result of one of the methods we compare: tetrahedral, unfolding, homotopy.

Empirical results shows the fast convergence using the power iteration method following the tetrahedral method.

D.3 MEMORY AND TIME REQUIREMENTS OF THE METHODS

General requirements:

Since our method consists on computing algebraic operations on tensors entries to store in matrix $n \times n$, the naive recovery method for a tensor of order k and for a tensor invariant of degree d would require $O(n^2)$ space requirements and $O(n^{kd})$ time complexity.

However, similarly to the matrix case where naive implementation requires n^3 but different methods propose better asymptotic bounds on the time required to multiply matrices, it is possible to simplify the computations by using decomposition on blocks (Ma et al. (2013)). There has been recently encouraging research investigating the optimization of tensor contractions (Kim et al. (2018), Matthews (2018),Huang et al. (2018)) in the same way it was done for matrix calculations, especially with the rise of the use of tensorial objects. The ability to be parallelized (each component of the matrix $\boldsymbol{M}_{\mathcal{G},e}$ can be computed independently) is also an important feature of our methods for practical applications.

Tetrahedral method with $\tilde{O}(n^4)$ time and $\tilde{O}(n^3)$ space requirement:

The unfolding algorithm (melonic) was proven to have a nearly linear time ($\tilde{O}(n^3)$, since the input tensor is of size n^3, $\tilde{O}$ notation neglects logarithmic factors).

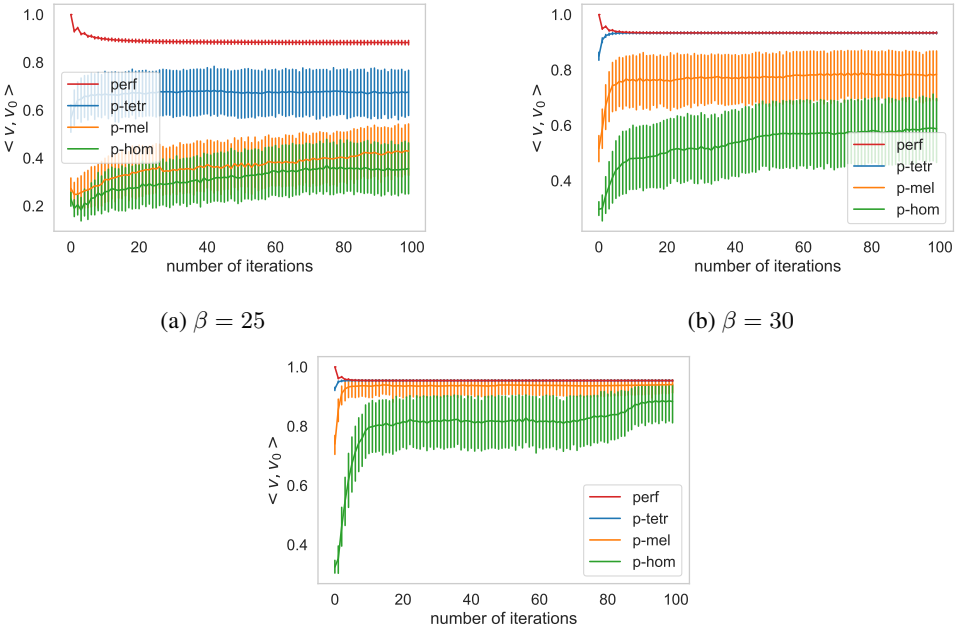

(a) $\beta = 25$

(b) $\beta = 30$

(c) $\beta = 35$

Figure 13: Correlation with the signal vector in function of the number of iterations of the power iteration for $n = 100$

We use a similar approach to provide a recovery algorithm for the tetrahedral with $\tilde{O}(n^4)$ time and $\tilde{O}(n^3)$ space requirement.

Indeed, using the decomposition 3, we can prove that there is an gap between the highest eigenvalue $\lambda_1 \sim \beta^4$ and the second largest one λ_2. Thus, we can use matrix power method in order to recover the leading eigenvector $\boldsymbol{v} \leftarrow \boldsymbol{M}^t \boldsymbol{v}$ with $\log(n)$ complexity (the convergence of the matrix power method is geometric with ratio $|\lambda_1/\lambda_2|$).

This lets us calculate the leading eigenvector of the matrix associated to the tetrahedral: $M^t_{i_1 i_2} \equiv \mathsf{T}_{i_1 jk} \mathsf{T}_{i_2 j'k'} \mathsf{T}_{ij'k} \mathsf{T}_{ijk'}$.

We can compute find the leading eigenvector in a time of $\tilde{O}(n^4)$ and space $\tilde{O}(n^3)$. Indeed each iteration of the matrix power iteration method requires two intermediate matrices we denote $\boldsymbol{A}, \boldsymbol{B}$ and a intermediate $3-$dimensional tensor we denote $\mathbf{C}$, in every step there is at most n^4 operations. we follow these steps:

- We take an initial vector $\boldsymbol{v}$
- We compute the matrix $\boldsymbol{A}$ defined as $A_{j'k'} \equiv \mathsf{T}_{i_2 j'k'} v_{i_2}$
- We compute the tensor $\mathbf{C}$ defined as $\mathsf{C}_{k'ik} \equiv A_{j'k'} \mathsf{T}_{ij'k}$
- We compute the matrix $\boldsymbol{B}$ defined as as $B_{kj} \equiv \mathsf{C}_{k'ik} \mathsf{T}_{ijk'}$
- Return the vector $\boldsymbol{v}'$ defined as $v'_{i_1} \equiv B_{kj} \mathsf{T}_{i_1 jk}$

Comparison between different methods

We use our results and the results reported in Anandkumar et al. (2017) to fill the Table 1. $\tilde{O}$ and $\tilde{\Omega}$ notation ignores logarithmic factors.

We plot the empirical time requirement of each method using Python in Figure 14a. However, to have a more accurate estimation of the time requirement, one has to take into account time to read the input (a tensor of size n^3). We obtain in this case Figure 14b.

Table 1: algorithmic threshold, time and space requirements for each method

Method	Time	Space	Threshold
Melonic detection	$O(n^3)$	$O(1)$	$\Omega(n^{3/4})$
Melonic recovery /Unfolding	$O(n^3)$	$O(n^2)$	$\Omega(n^{3/4})$
Tetrahedral recovery	$O(n^4)$	$O(n^3)$	$\Omega(n^{3/4})$
Sum of squares	$> \Omega(n^6)$	$> \Omega(n^6)$	$\tilde{\Omega}(n^{3/4})$
Homotopy	$O(n^3)$	$O(n)$	$\Omega(n^{3/4})$
Information-theoretic	Exp	$O(n)$	$\tilde{\Omega}(n^{1/2})$

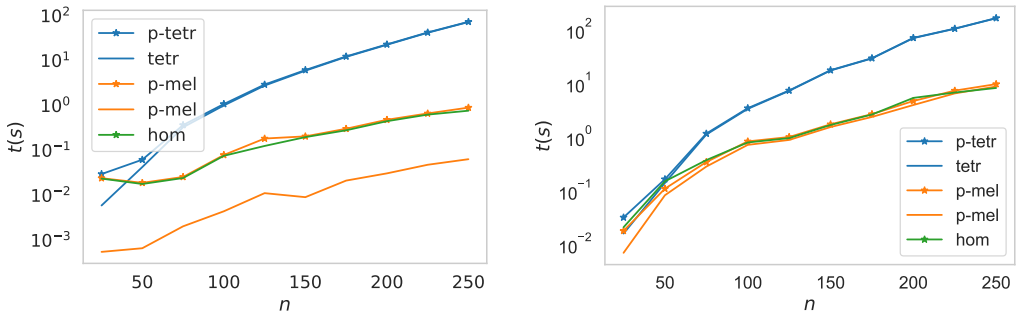

(a) without taking into account the input reading

(b) with taking into account the input reading

Figure 14: Empirical time requirement for different methods in function of n without and with taking into account the input reading

D.4 Different dimensions

D.4.1 The settings

Each experiment is an independent instance consisting in the following steps:

- We generate randomly the n components of the signal vectors $\boldsymbol{v}_1$, $\boldsymbol{v}_2$ and $\boldsymbol{v}_3$ and then normalize them.
- We generate randomly the n^3 components of the random tensor $\mathbf{Z}$.
- We compute the tensor $\mathbf{T} = \mathbf{Z} + \beta \boldsymbol{v}_1 \otimes \boldsymbol{v}_2 \otimes \boldsymbol{v}_3$
- We compute the three matrices to recover each of the vectors by opening an edge of the color corresponding to the position of the vector using the numpy method tensordot in Python.
- We compute their leading eigenvectors.
- We plot the correlation between the vector resulted from the algorithm and the signal vectors we aim to recover $\boldsymbol{v}_1$, $\boldsymbol{v}_2$ and $\boldsymbol{v}_3$ (namely scalar product $< \boldsymbol{v}, \boldsymbol{v}_i >$).

We see in the Figure 15 that when $n_3 > n_1 n_2$, the asymptotic behavior of the recovery threshold of v_3 matches with our theoretical result $n_3^{1/2}$

D.5 Multiple spikes

We choose to take the β_i equal since we expect it to be the hardest case (it is more difficult to distinguish the spikes). Each experiment is an independent instance consisting in the following steps:

- We generate randomly the p orthogonal vectors $\boldsymbol{v}_i$ and then normalize them.

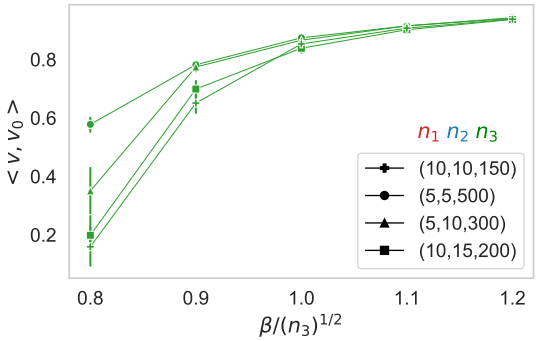

Figure 15: Recovery of $\boldsymbol{v}_3$ where $n_3 > n_1 n_2$

  - Generate the components of $\boldsymbol{v}_i$ randomly.
  - $\forall j \in [i]$ we compute $\boldsymbol{v}_i \leftarrow \boldsymbol{v}_i - \langle \boldsymbol{v}_i, \boldsymbol{v}_j \rangle \boldsymbol{v}_j$ in order to have orthogonal spikes.
  - Normalize $\boldsymbol{v}_i$
- We generate randomly the n^3 components of the random tensor $\mathbf{Z}$.
- We compute the tensor $\mathbf{T} = \mathbf{Z} + \sum_i \beta_i \boldsymbol{v}_i^{\otimes 3}$
- We compute the matrix associated to the tetrahedral with the numpy method tensordot in Python.
- We compute its eigenvectors $\boldsymbol{x}_i$.
- We iterate the following steps beginning from $i = 0$ to $i = p$:
  - We use the power iteration method on $\boldsymbol{x}_i$ with 100 iterations.
  - We update the tensor $\mathbf{T} \leftarrow \mathbf{T} - \alpha_i \boldsymbol{x}_i^{\otimes 3}$ where $\alpha_i = T_{jkl} (\boldsymbol{x}_i)_j (\boldsymbol{x}_i)_k (\boldsymbol{x}_i)_l$
- Since the vectors $\boldsymbol{x}_i$ are not necessarily ordered, we want to make a one for one correspondence with the vectors $\boldsymbol{v}_i$. So for $\boldsymbol{v}_1$, we search for the $\boldsymbol{x}_j$ that maximizes $\langle \boldsymbol{x}_j, \boldsymbol{v}_i \rangle$. We call rename it $\boldsymbol{w}_i$. Then for the other $\boldsymbol{v}_i$ we search for the $\boldsymbol{x}_j$ that maximizes $\langle \boldsymbol{x}_j, \boldsymbol{v}_i \rangle$ in the set $X = \{\boldsymbol{x}_j,\ j \in [p]\} \setminus \{\boldsymbol{w}_k,\ k \in [i-1]\}$. In that way, for each $\boldsymbol{v}_i$ there is a one to one correspondence to a vector $\boldsymbol{x}_j$ that we rename $\boldsymbol{w}_i$.
- We plot the correlation between the vectors resulted from the algorithm w_i and the signal vectors we aim to recover $\boldsymbol{v}_i$ (namely scalar product $\langle \boldsymbol{w}_i, \boldsymbol{v}_i \rangle$) for each i.

We see that empirically, our method is able to recover any number of spikes inferior to n, and with a similar threshold than with a single spike.

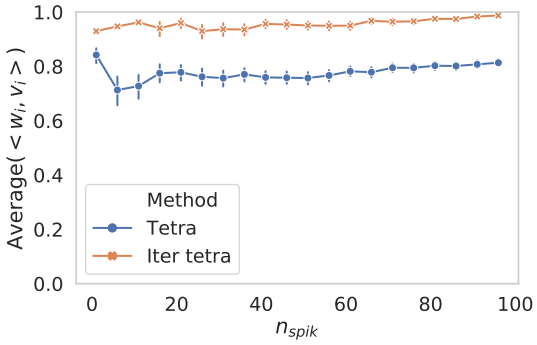

Figure 16: Average of the correlation of the recovered vector with their corresponding signal vector in function of the number of spikes for $n = 100$ and $\beta = 30$

We see that when the spacing between the β_i gets bigger, it is easier to retrieve the signal vectors, since it will be easier to distinguish them. Thus the case where all β_i are equal is the hardest case.

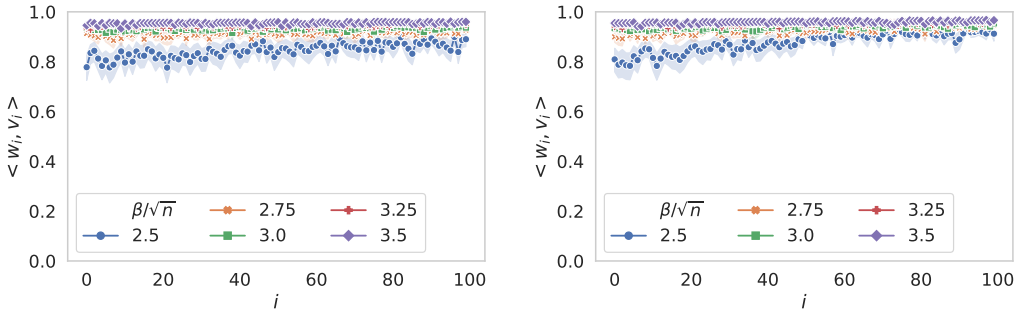

(a) Recovery many spikes with $\beta_i = \beta + 0.02i$

(b) Recovery many spikes with $\beta_i = \beta + 0.05i$

Figure 17: Recovery of many spikes with non equal β_i

E PROOFS

We begin by giving useful lemmas and definitions that will be used in the proofs.

Decomposition graphs:

Let's decompose a tensor invariant $I_{\mathcal{G}}(\mathbf{T})$ of degree d using the graphical decomposition of the Figure 3 of $\mathbf{T} = \mathbf{Z} + \beta \boldsymbol{v}^{\otimes k}$. In each of the graphs illustrating the decomposition (like in Figure 4), we call each vertex: a spike vertex if it corresponds to the spike tensor $\boldsymbol{v}^{\otimes 3}$ and a pure noise vertex if it corresponds to the random tensor $\mathbf{Z}$. This leads us to denote the graphs illustrating the decomposition of the tensor invariant (that we will call the decomposition graphs):

- The pure noise graph: the graph where all the vertices are replaced by pure noise vertices. It gives a contribution of $I_{\mathcal{G}}(\mathbf{Z})$.
- The pure signal graph: the graph where all the vertices are spike vertices. It gives a contribution of β^d.
- The intermediate graphs: All the other graphs, which have pure noise vertices **and** spike vertices.

We define in a similar way the pure noise, pure signal and the intermediate matrices for the decomposition of a matrix $\boldsymbol{M}_{\mathcal{G},e}$.

We call the expectation and the variance of a graph, the expectation and variance of the tensor invariant associated to it. In particular, in the case of a pure noise graph, the variance will be the Gaussian variance defined in the end of Section 2.4.

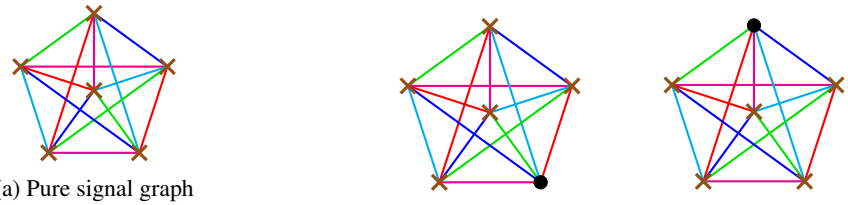

(a) Pure signal graph

Figure 18: Example of a pure signal graph in the left and of intermediate graphs in the right

Operator norm of a matrix:

In our proofs we will use Wedin perturbation theorem in order to compute the recovery threshold. This theorem requires computing the operator norm of a matrix $\boldsymbol{M}_{\mathcal{G},e}$ that will be in our case associated to a graph $\mathcal{G}$ and an edge e.

Let $\boldsymbol{A} \in \mathbb{C}^{n \times n}$ be a matrix and $\lambda_1, \ldots, \lambda_n$ its (real or complex) eigenvalues. The spectral radius of $\boldsymbol{A}$ is its highest eigenvalue in absolute value. In particular, when a matrix $\boldsymbol{A}$ is symmetric, we have the result $\rho(\boldsymbol{A}) = \|\boldsymbol{A}\|_{\text{op}}$. Thus, in order to compute the operator norm of a given matrix $\boldsymbol{M}$, we can determine the spectral radius of the symmetric matrix $\boldsymbol{A} \equiv \boldsymbol{M}^\top \boldsymbol{M}$ and take its square root since $\left\|\boldsymbol{A}^\top \boldsymbol{A}\right\|_{\text{op}} = \|\boldsymbol{A}\|_{\text{op}}^2$.

In order to compute the spectral radius of $\boldsymbol{A} \equiv \boldsymbol{M}^\top \boldsymbol{M}$, we use Gelfand's Formula with the Frobenius norm. Thus computing the operator norm of $\boldsymbol{M}$ is equivalent to calculating

$$\|\boldsymbol{M}\|_\infty = \lim_{r \to \infty} \mathrm{Tr}\big((\boldsymbol{M}^\top \boldsymbol{M})^r\big)^{1/2r} \tag{14}$$

The graph used to investigate the operator norm of a matrix

Let $\boldsymbol{A} = \boldsymbol{M}_{\mathcal{G},e}^\top \boldsymbol{M}_{\mathcal{G},e}$ where $\boldsymbol{M}_{\mathcal{G},e}$ is the matrix associated to a graph $\mathcal{G}$ and an edge e. The trace of the power r of $\boldsymbol{A}$, $\mathrm{Tr}(\boldsymbol{A}^r)$ can be represented as the graph gluing the open edges of $2r$ subgraphs $\mathcal{G}'$ where $\mathcal{G}'$ is the graph $\mathcal{G}$ with the edge e open, that represents the matrix $\boldsymbol{M}_{\mathcal{G},e}$. We denote the total graph representing $\mathrm{Trace}(\boldsymbol{A}^r)$ by $\mathcal{G}^{tot}$.

Elementary subgraph We call the elementary subgraphs of $\mathcal{G}^{tot}$ representing $\mathrm{Tr}\big((\boldsymbol{M}^\top \boldsymbol{M})^r\big)$ the subgraph corresponding to a single matrix $\boldsymbol{M}$. Thus $\mathcal{G}^{tot}$ consists in gluing together $2r$ elementary graphs, like in Figure 19.

Internal propagator: We call a propagator of a covering graph an internal propagator if it connects two vertices of the same elementary subgraph.

Comparison of the contributions of the graphs and of the matrices We say that a graph $\mathcal{G}_1$ have a much larger contribution than a graph $\mathcal{G}_2$ if $\lim_{n\to\infty} I_{\mathcal{G}_2}/I_{\mathcal{G}_1} = 0$ with high probability. In particular, using Chebyshev inequality, we know that this is the case if $\mathbb{E}((I_{\mathcal{G}_1}(\mathbf{T}))^2) \gg \mathbb{E}((I_{\mathcal{G}_2}(\mathbf{T}))^2)$ in the large n limit. We use the same notations in the case of matrices, where we compare the operator norms, which is equivalent to comparing the contributions of the graphs $\mathrm{Tr}\big((M^\top M)^r\big)$.

It should be noted that the graph associated to $(I_{\mathcal{G}}(\mathbf{T}))^2$ is the graph made of two disconnected copies of $\mathcal{G}$.

Claim of the proofs: As mentioned in the main text, our results hold for the large n limit, and the experimental results suggest that the approximation of large n limit is valid for $n \geq 25$. We claim that an event X occurs with high probability if Probability$(X) \to 1$ when $n \to \infty$.

Simplification of the notations: In the remainder of this section, we will assume that the matrix is symmetric to simplify the notations. One should keep in mind that if the matrix is not symmetric, we have to consider $\boldsymbol{A} = \boldsymbol{M}^\top \boldsymbol{M}$ instead of just $\boldsymbol{M}$, which affect only the notations in the proofs.

Some useful lemmas:

Lemma 10. *The covering graphs involved in the calculation of $E(\mathrm{Tr}(\boldsymbol{M} - \mathbb{E}(\boldsymbol{M}))^r)$ are the same that are involved in the calculation of $E(\mathrm{Tr}(\boldsymbol{M}^r))$ minus the covering graphs where one of the elementary subgraphs has only internal propagators.*

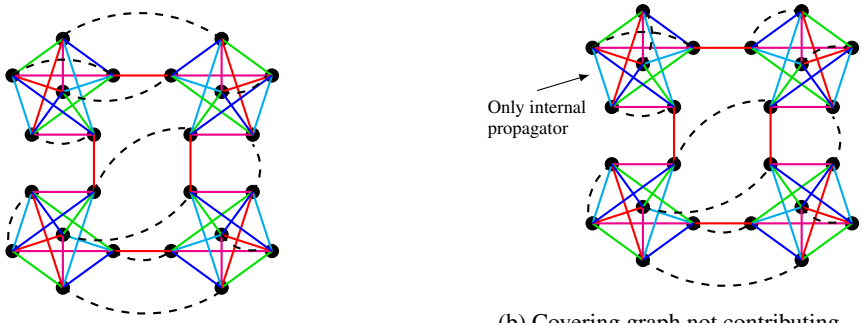

(a) Covering graph contributing

(b) Covering graph not contributing to $\mathbb{E}(\mathrm{Tr}\big((\boldsymbol{M} - \mathbb{E}(\boldsymbol{M}))^2\big))$

Figure 19: Two covering graphs for the graph of $\mathrm{Tr}\big((\boldsymbol{M}^\top \boldsymbol{M})^2\big)$

Lemma 11. *If $\beta_{det} = \mathcal{O}(n^{3/4})$ for a graph $\mathcal{G}$, the contributions of the intermediate graphs and the intermediate matrices (its operator norm) associated to $\mathcal{G}$ contributions are negligible comparing to either the pure noise or the pure signal.*

It means that if we want to investigate the recovery when $\beta_{\text{det}} = \mathcal{O}(n^{3/4})$, we can disregard the intermediate matrices since their operator norm is always much smaller than the pure noise matrix or the pure signal matrix operator norm.

Proof of Lemma 1 Let $\boldsymbol{M}$ be the matrix obtained by cuting the edge e of a trace invariant graph $\mathcal{G}$. We know that the equation 9 identify the indices i and j that are ends of a same edge by including a factor δ_{ij}. Hence, the non diagonal components $M_{ij},\ i \neq j$ have a null expectation since the cycle involving the edge e will identify i and j with a $\delta_{ij} = 0$. By invariance, $\{\mathbb{E}(M_{ii})\}_{i\in[n]}$ are all equal. Then, by linearity of the expectation, $\mathbb{E}(M_{ii}) = \mathbb{E}(\mathrm{Tr}(\boldsymbol{M}))/n = \mathbb{E}(\mathcal{G})/n$.

(a) Example of a covering graph

(b) The cycle containing the open edge contributing by δ_{ij}

Figure 20: Cycle with an open edge

Proof of theorem 2 The idea of this theorem is that detecting a signal in a tensor $\mathbf{T}$ could be done through calculating the invariant $I_{\mathcal{G}}(\mathbf{T})$ associated to $\mathcal{G}$ of $\mathbf{T}$. Then one compares it to the distribution of this invariant for a pure noise tensor, that is $\mathbb{E}(I_{\mathcal{G}}(\mathbf{B}))$ and $\sigma(I_{\mathcal{G}}(\mathbf{B}))$ where the components of $\mathbf{B}$ are Gaussian random.

Let $n \in \mathbb{N}$ and $\mathcal{G}$ a graph of degree d. When considering the decomposition graphs, each graph will have a contribution which is proportional to β to the power the number of spike vertices the graph has:

- Pure signal graph has a contribution strictly equal to β^d.
- Intermediate graphs with $d-1$ spike vertices and 1 pure noise vertex. Their contributions have an expectation equal to zero and a variance $\propto \beta^{d-1}$.
- Intermediate graphs with $d-2$ spike vertices and 2 random tensor vertices. Their expectation and variance will be $\propto \beta^{d-2}$
- etc.

Thus in the limit $\beta \to \infty$, the graph with the largest contribution will be the pure signal tensor, with a value of β^d, this will give the expectation of the tensor invariant $I_{\mathcal{G}}(\mathbf{T})$. The second largest ones will be the intermediate graphs with $d-1$ spike vertices, with a contribution proportional to $\beta^{(d-1)}$. So in this limit we have: $\mathbb{E}(I_{\mathcal{G}}(\mathbf{T})) \sim \beta^d$ while $\sigma(I_{\mathcal{G}}(\mathbf{T})) \sim \beta^{(d-1)}$.

Then, a direct application of Chebyshev's inequality demonstrates that the distributions of $I_{\mathcal{G}}(\mathbf{T})$, $\beta \to \infty$ and $I_{\mathcal{G}}(\mathbf{B})$ (where the components of $\mathbf{B}$ are Gaussian random) are disjoint with high probability, like in Figure 21, which allow the detection of a signal. Thus, $\exists \beta_{\text{det}}$ such that $\forall \beta \geq \beta_{\text{det}}$, the detection is possible.

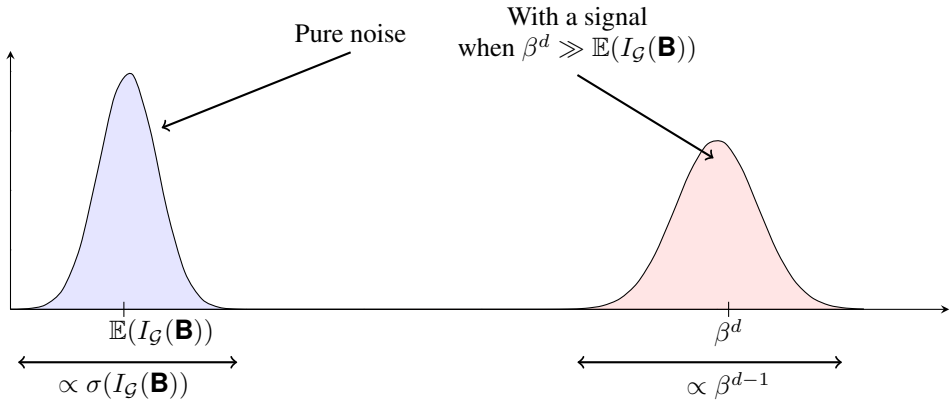

Figure 21: The pure noise and strong signal distributions of an invariant $I_{\mathcal{G}}(\mathbf{T})$ of degree d

Proof of theorem 3 Let $n \in \mathbb{N}$, $\mathcal{G}$ a graph of degree d and $\boldsymbol{M}_{\mathcal{G},e}$ the matrix obtained by cutting the edge e. As explained in the beginning of the appendix, studying the operator norm comes down

to studying the graph $\mathrm{Tr}(M^r)$. Thus we can use a similar demonstration to the previous proof. Therefore, when $\beta \to \infty$ for a fixed n, the matrix with the largest operator norm will be the one where all the vertices are spike vertices, and which is proportional to $\boldsymbol{v}\boldsymbol{v}^T$. Then applying Wedin perturbation theorem proves that $\exists \beta_{\text{rec}}$ such that $\forall \beta \geq \beta_{\text{rec}}$, the recovery is possible.

Proof of theorem 4 We aim to prove that $\mathbb{E}((I_{\mathcal{G}})^2) \geq n^{dk/2}$. As previsouly noted, the graph corresponding to the invariant $(I_{\mathcal{G}})^2$ consists in two copies of $\mathcal{G}$ that we denote $(\mathcal{G})^2$, as in Figure 22. A simple way to prove our claim, is to exhibit for any graph $\mathcal{G}$ a covering graph for $(\mathcal{G})^2$ that gives a contribution of $n^{dk/2}$. Such a covering graph is obtained by connecting each vertex of $\mathcal{G}$ to its equivalent in the second copy as shown in Figure 22. All the cycles for the colors $0, c$ will be of length 2 (consisting in an edge and its equivalent in the other copy). Their total number is equal to $dk/2$, so this covering graph gives a contribution equal to $n^{dk/2}$. Since the expectation is equal to the sum of the contributions of the covering graphs, the variance will always be larger than $n^{dk/4}$. A similar argument proves that the variance of $\mathrm{Tr}\big((MM^T)^r\big)$ will be always superior to $n^{rd/2}$.

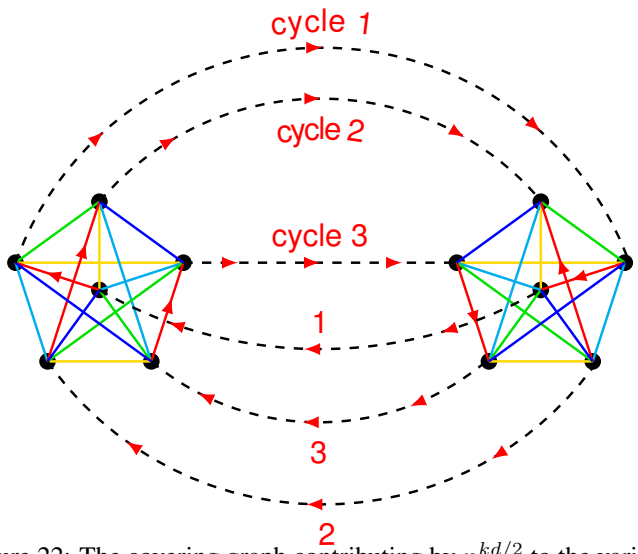

Figure 22: The covering graph contributing by $n^{kd/2}$ to the variance

Proof of theorem 5 : We will use the lemma 10.

Let's prove by induction that $\mathbb{E}(\mathrm{Tr}\big((MM^T)^r\big)) \leq n^{kr+1}$ where M is the matrix associated to the melon by opening one of its edge.

For $r = 1$ it is straightforward by simply enumerating the cycles. Now, let $r > 1$ and let's assume the statement is true for all $r' < r$. Let's consider one of its elementary subgraphs (defined in the beginning of the section). Using lemma 10, we can divide the edges of the subgraph in two sets:

- $k - 1$ edges that are in faces of at least two edges.
- One external edge divided in half edges.

If the $k - 1$ edges are in faces of exactly two edges, itt means that the propagators at both the left and right vertices are connected to the vertices of the same other elementary subgraph.

This will lead to two possibilities:

- The two elementary subgraphs are next to each other. Then we remove these two elementary subgraphs and connect the two left open edges. We will have a contribution of n^k from the two elementary subgraphs and use the induction hypothesis to show that the remaining graph has a contribution of maximum $n^{k(r-1)+1}$. Combining them we have a total contribution of $n^{k(r-1)+1+k} = n^{kr+1}$ which proves the theorem.

- The two subgraphs are not next to each other: Then the open edges have also a contribution of maximum $1/2$. Cutting this elementary subgraph and using the induction hypothesis proves the theorem.

Thus using Gelfand's Formula, the norm operator is equal to $n^{3/2}$. Which gives a recovery threshold for the melon of $\beta = n^{3/4}$ using Wedin perturbation.

For the symmetric case, since $T^{sym}_{ijk} = \sum_{\tau \in \mathfrak{S}_k} T_{\tau(i)\tau(j)\tau(k)}$ where $\mathfrak{S}_k$ is the symmetric group introduced previously. We just need to expand the melonic matrix $T^{sym}_{i_1jk} T^{sym}_{i_2jk}$ in function of the asymmetric tensor $\mathbf{T}$. We obtain a sum of nine matrices (corresponding to graphs with mixed colors). We can show that the operator norm of each of these matrices is at most equal to $n^{3/2}$.

Proof of theorem 6 : Using the matrix decomposition illustrated in 23, we can see that we have a sum of four matrices of rank one. Using the usual formula to calculate the expectation of the operator norm of the matrices we obtain:

- $\left\| \boldsymbol{M}^{(N)} \right\| = n^2$
- $\left\| \boldsymbol{M}^{(D)} \right\| = n$
- $\left\| \boldsymbol{M}^{(R)} \right\| = n^{3/2}$

we can see that the first one dominates by $n^{1/4}$ the last one (consisting in the signal vector) so we are able to use power iteration or one of its variants (like in Anandkumar et al. (2017) and Biroli et al. (2020)) to recover it.

$$\boldsymbol{M}_{\mathbf{i}_1\mathbf{i}_2} = \boldsymbol{M}^{(N)}_{\mathbf{i}_1\mathbf{i}_2} + \boldsymbol{M}^{(D)}_{\mathbf{i}_1\mathbf{i}_2} + \boldsymbol{M}^{(R)}_{\mathbf{i}_1\mathbf{i}_2}$$

$$= \mathbf{Z}_{\mathbf{i}_1\mathbf{j}\mathbf{j}}\mathbf{Z}_{\mathbf{i}_2\mathbf{k}\mathbf{k}} + \beta\ (\boldsymbol{v}_{\mathbf{i}_1}\mathbf{Z}_{\mathbf{i}_2\mathbf{k}\mathbf{k}} + \boldsymbol{v}_{\mathbf{i}_2}\mathbf{Z}_{\mathbf{i}_1\mathbf{j}\mathbf{j}}) + \beta^2\boldsymbol{v}_{\mathbf{i}_1}\boldsymbol{v}_{\mathbf{i}_2}$$

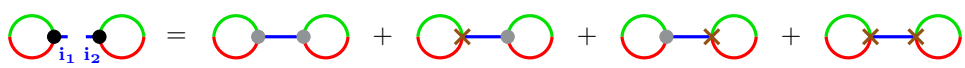

Figure 23: Decomposition of a tadpole matrix

Proof of theorem 7 : Let's define a set of even numbers $(s_i)_{i \in \{0,\dots,r\}}$ where $s_i/2$ is equal to the number of propagators having its two vertices in the subgraph G_i (we call these propagators internal). Thus we have $s/2 \equiv= \sum_i s_i/2$ internal propagators in total. We can divide the edges of the subgraph $\mathcal{G}$ in three classes. Each edge could be part of a face of either one edge, two edges, three edges, etc.. Let's count how many we can have of each type in an optimal configuration (maximizing the number of faces) for each class.

- Edges only connected to internal propagators, there is at most $\sum_i s_i(s_i-1)/2$ such edges.
  - We can have a maximum of $s_i/2$ faces of one edge since that is the number of internal edges.
  - Then, from the $s_i(s_i-2)/2$ remaining ones, if we want to put them in faces of two edges, the two edges needs too to be in the same subgraph. Thus, we can create a maximum of $s_i/2(s_i/2-1)/2 = s_i(s_i-2)/8$ different couples of propagators. Each couple can't create more than one face since otherwise it will contradict the maximally single trace hypothesis of the graph. So there is a maximum of $s_i(s_i-2)/4$ edges that can be put in two edges faces.
  - The remaining $s_i(s_i-2)/4$ will be in faces of at least three edges.
- Edges connected to one internal and one external propagators, there is at most $\sum_i s_i(k+1-s_i)$ one such edges. They can only be in faces of at least three edges.
- Edges only connected to external propagators, there is at most $\sum_i ((k+1-s_i)(k-s_i)/2)$ such edges. They can only be put in faces of at least two edges.

- The open edge can be put in a face of maximum one edge.

So we have a maximal number of faces given by:

$$\begin{aligned}&\sum_{i=1}^{r}\left(\frac{s_i}{2}+\frac{s_i(s_i-2)}{8}+\frac{s_i(s_i-2)}{12}+\frac{s_i(k+1-s_i)}{3}+\frac{(k+1-s_i)(k-s_i)-2}{4}+1\right)\\=&\sum_{i=1}^{r}\left(\frac{k(k+1)}{4}-s_i\frac{4k-3s_i-4}{24}+\frac{1}{2}\right).\end{aligned}\tag{15}$$

Let's focus in the case where $s_i = 0$. If all the points of the graph are connected to points of another graph, then the two extremes of the open edge connects to the same graph. In that case the open edge has a contribution of only $1/2$. In the other case, then there is at least k edges which contributes only by at most $1/3$ making them lose $1/6$. Either way the contribution of the subgraph can't go further then $k(k+1)/4$. We obtain:

$$\sum_{i=1}^{r}\left(\frac{k(k+1)}{4}-s_i\frac{4k-3s_i-4}{24}+\frac{1-\delta_{s_i,0}}{2}\right).\tag{16}$$

We can easily check that this quantity is always smaller than $\frac{k(k+1)}{4}$ for $k > 5$.

Proof of theorem 8 : Let's consider the melonic graph with the edge associated to the index of the space of dimension n_l open. It is associated to the matrix:

$$M_{pq} = \mathsf{T}_{i_1\dots i_{l-1}pi_{l+1}\dots i_k}\,\mathsf{T}_{i_1\dots i_{l-1}qi_{l+1}\dots i_k}\tag{17}$$

For simplicity the graphs will be drawn for $k = 3$.

We will treat two separate cases:

- Case $n_l \leq \prod_{i\neq l} n_i$:

  Let's prove by induction the statement: S_r: $\mathbb{E}[\mathrm{Tr}((\boldsymbol{M}-\mathbb{E}(\boldsymbol{M}))^r)] \sim n_l \prod_{i=1}^{k} n_i^{r/2}$.

  - Initialisation with $r = 2$: For $\boldsymbol{M}-\mathbb{E}(\boldsymbol{M})$ we have the following graph and its covering graphs:

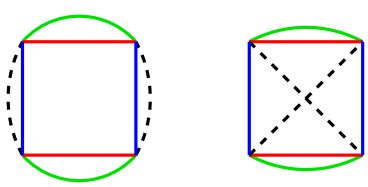

Figure 24: The two covering graphs of $\mathrm{Tr}\big(M^2\big)$

    which gives

$$\mathbb{E}(\mathrm{Tr}(M^r) = n_l\prod_{i=1}^{k} n_i + \prod_{i=1}^{k} n_i \leq 2n_l\prod_{i=1}^{k} n_i^{r/2}$$

  - Assume S_r is true for all $r' < r$, let's prove for r that no covering graph has a contribution strictly superior to $n_l \prod_{i=1}^{k} n_i^{r/2}$ and then that we can provide a covering graph that contribute by exactly $n_l \prod_{i=1}^{k} n_i^{r/2}$.
    * In the case where there is no cycle of color l of length 1 (which means a propagator that shares the same ends that an edge of color l), then all edges have a contribution of $1/2$ at maximum. So the contribution of that covering graph will be at most equal to $\prod_{i=1}^{k} n_i^{r/2}$.

* In case there is such a propagator, which means that there is a propagator coinciding with an edge of color l between two elementary subgraphs. Let r Then either the two other ends of the two elementary subgraphs are connected by a propagator like in 25 or not. In the first case, the total number of cycles will be at most equal to one cycle of each color, plus the number of cycles of a graph with $r-2$ elementary subgraphs, which is $n_l \prod_{i=1}^{k} n_i^{r/2}$
* The covering graph consisting in propagators like in Figure 25 (left) will give a contribution of exactly $n_l \prod_{i=1}^{k} n_i^{r/2}$

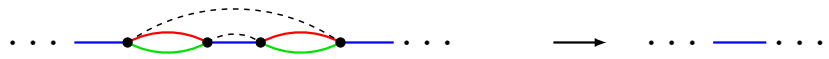

Figure 25: Elementary subgraphs connecting to the ementary subgraph next to it

* In the second case, we can remove the cycle of one edge of color l and mix the two elementary subgraphs adjacent to it into one, we use then the induction hypothesis to show that Which proves the statement.

Figure 26: Elementary subgraphs connecting to the ementary subgraph next to it

- Case $n_l \geq \prod_{i \neq l} n_i$:

  Let's prove by induction the statement: S_r: $\mathbb{E}[\mathrm{Tr}((\boldsymbol{M}-\mathbb{E}(\boldsymbol{M}))^r)] \sim n_l^r \prod_{i \neq l} n_i$.

  - Initialisation with $r=2$: For $\boldsymbol{M}-\mathbb{E}(\boldsymbol{M})$ we have the covering graphs in Figure 24 which checks S_2
  - Assume S_r is true for all $r' < r$, let's prove for r that no covering graph has a contribution strictly superior to $n_l^r \prod_{i \neq l} n_i$ and then that we can provide a covering graph that contribute by exactly $n_l^r \prod_{i \neq l} n_i$.
    * In the case where there is no cycle of color l of length 1 (which means a propagator that shares the same ends that an edge of color l), then all edges have a contribution of $1/2$ at maximum. So the contribution of that covering graph will be at most equal to $\prod_{i=1}^{k} n_i^{r/2}$.
    * In case there is such a propagator, which means that there is a propagator coinciding with an edge of color l between two elementary subgraphs. Then either the two other ends of the two elementary subgraphs are connected by a propagator like in Figure 25 or not. In the first case, the total number of cycles will be at most equal to one cycle of each color, plus the number of cycles of a graph with $r-2$ elementary subgraphs, so the contribution of the covering graph will be at most $n_l^{r-2} \prod_{i \neq l} n_i \times \prod_{i=1}^{k} n_i$, which is smaller than $n_l^r \prod_{i \neq l} n_i$. In the second case (the case of Figure 26), by induction the number of cycles will be at most the one of $r-1$ elementary subgraph plus a cycle of color blue. Thus, it is at most equal to $n_l^r \prod_{i \neq l} n_i$.
    * The covering graph consisting in propagators coinciding with blue edges has a contribution exactly equal to $n_l^r \prod_{i \neq l} n_i$.

Proof of theorem 9 : Let $\tilde{\boldsymbol{A}} = \boldsymbol{M}_{\mathcal{G}}^{e}(\mathbf{T})$ the matrix we have with noise and $\boldsymbol{A} = \sum_{i=1}^{p} \beta_i^d \boldsymbol{v}_i^k$ the matrix when there is no noise and only signal. We call an eigenspace of $\boldsymbol{A}$ the subspace of $\mathbb{R}^n$ spanned by some eigenvectors of $\boldsymbol{A}$.

The idea of the proof of the theorem is that for β large enough, the eigenspace spanned by the signal vectors S should be close to the eigenspace spanned by the p largest eigenvectors of $\tilde{\boldsymbol{A}}$ denoted $\tilde{S}$.

Then, we take a vector from this subspace $\tilde{S}$, we perform power iteration on it in order to recover a signal vector w_1, and repeat this step by restricting to the subspace of $\tilde{S}$ orthogonal to w_1.

If there were only one signal, there is a simple way to calculate how close are v_1 and w_1: $\theta(v_1, w_1) = \cos^{-1}(v_1.w_1)$. To quantify the closeness of two subspaces S and $\tilde{S}$, we use the canonical angles. The first canonical angle is defined as follow:

$$\theta_1 = \cos^{-1}(\max_{\substack{x \in S \\ \|x\|=1}} \max_{\substack{y \in \tilde{S} \\ \|y\|=1}} |x.y|) = \cos^{-1}(x_1.y_1) \tag{18}$$

where we denoted the maximizers by x_1 and y_1 and $x.y$ denotes the scalar product between x and y.

Then we define by iteration the kth canonical angle by:

$$\theta_k = \cos^{-1}(\max_{\substack{x \in S \\ \|x\|=1 \\ x.x^{k'}=0 \\ \forall k' \in \{1,\dots,k-1\}}} \max_{\substack{y \in \tilde{S} \\ \|y\|=1 \\ y.y^{k'}=0 \\ \forall k' \in \{1,\dots,k-1\}}} |x.y|) = \cos^{-1}(x_k.y_k) \tag{19}$$

We put these angles in a matrix Θ

$$\Theta = \begin{pmatrix} \theta_1 & \dots & 0 \\ \vdots & \ddots & \vdots \\ 0 & \dots & \theta_r \end{pmatrix} \tag{20}$$

We define now the distance between S and $\tilde{S}$ by $\|\sin(\Theta)\|_F$ with $\sin(\Theta)$ defined as:

$$\sin(\Theta) = \begin{pmatrix} \sin(\theta_1) & \dots & 0 \\ \vdots & \ddots & \vdots \\ 0 & \dots & \sin(\theta_r) \end{pmatrix} \tag{21}$$

The Davis-Kahan Theorem uses these tools to provide a bound on subpaces spanned by eigenvectors under perturbation (Stewart & guang Sun (1990)):

Davis-Kahan: Let $\boldsymbol{A}$, $\boldsymbol{A}'$ two symmetric matrices with respective eigenvectors:

$$\lambda_1 \geq \lambda_2 \geq \dots \geq \lambda_r$$
$$\tilde{\lambda}_1 \geq \tilde{\lambda}_2 \geq \dots \geq \tilde{\lambda}_r$$

Let's define the eigengap as:

$$\delta = \inf\{\left|\lambda - \tilde{\lambda}\right| : \lambda \in [\lambda_s, \lambda_r], \tilde{\lambda} \in (-\infty, \tilde{\lambda}_{s+1}] \cup [\tilde{\lambda}_{s+1}, \infty)\} \tag{22}$$

Then if $\delta > 0$

$$\left\|\sin \Theta(S, \tilde{S})\right\|_F \leq \frac{\left\|\tilde{\boldsymbol{A}} - \boldsymbol{A}\right\|_F}{\delta} \tag{23}$$

The result also holds for $\|.\|_{\text{op}}$

Let's study the case where $\beta_d > cn^{k/4}$ where c is a constant large enough. The gap will be equal to $\delta = (c-1)n^{k/4}$. In the case of the melonic graph, $\left\|\tilde{\boldsymbol{A}} - \boldsymbol{A}\right\|_{op}$ can be bounded by $2n^{k/4}$. Let's take a vector z from $\tilde{S}$. It can be put in the form of:

$$\begin{aligned} z = \sum_{i=1}^{p} \alpha_i \boldsymbol{y}_i &= \sum_{i=1}^{p} \alpha_i \boldsymbol{x}_i + \alpha_0 \boldsymbol{q}' \\ &= \sum_{i=1}^{p} \gamma_i \boldsymbol{v}_i + \gamma_0 \boldsymbol{q} \end{aligned} \tag{24}$$

where $\boldsymbol{q}'$ and $\boldsymbol{q}$ are unitary vectors, and $\boldsymbol{q} = \boldsymbol{q}' - \sum_{i=1}^{p} (\boldsymbol{q}'.\boldsymbol{x}_k)\boldsymbol{x}_k$ so it is orthogonal to all the vectors $\boldsymbol{v}_i$ and that $|\gamma_0| \leq |\alpha_0|$. Let's put a high bound for $alpha_0$. Since $x_k.y_k = \cos(\theta_k),\ \forall k \in \{1, \ldots, p\}$

$$\begin{aligned} |\alpha_0| &= \left\| \sum_{i=1}^{p} \alpha_i \boldsymbol{y}_i - \sum_{i=1}^{p} \alpha_i \boldsymbol{x}_i \right\| \\ &\leq p \max_k |\sin(\theta_k)| \\ &\leq p \left\| \sin \Theta(S, \tilde{S}) \right\|_{\text{op}} \end{aligned} \tag{25}$$

Using these results, we show that power iteration on a vector z of S is able to recover a signal vector $\boldsymbol{v}_k$:

$$\begin{aligned} \mathsf{T}_{ijk} z_j z_k &= \left(\mathsf{Z}_{ijk} + \sum_l \beta_l \ \boldsymbol{v}_l^{\otimes k} \right) z_j z_k \\ &= \mathsf{Z}_{ijk} z_j z_k + \sum_l \beta_l \gamma_l^2 \ \boldsymbol{v}_l \end{aligned} \tag{26}$$

Thus, repeating $\boldsymbol{z} \leftarrow \mathbf{T}\boldsymbol{z}\boldsymbol{z}$ will converge to $\boldsymbol{v}_{l_{\max}}$ with $l_{\max} = \max(\{\beta_l \gamma_l^2, l \in \{1, \ldots, r\}\})$

We repeat this step p times, but before each step we use deflation by computing:

$$\mathbf{T} \leftarrow \mathbf{T} - (\mathbf{T}\boldsymbol{z}_k \boldsymbol{z}_k \boldsymbol{z}_k) \boldsymbol{z}_k^{\otimes k}$$

The deflation is used to avoid converging twice to the same vector. Since we take p a constant in the large n limit, the error bounds will remain very small and we are able to recover the p spikes.

Proof of Lemma 10 The covering graphs involved in the calculation of $E(\mathrm{Tr}(\boldsymbol{M} - \mathbb{E}(\boldsymbol{M}))^r)$ are the same that are involved in the calculation of $E(\mathrm{Tr}(\boldsymbol{M}^r))$ minus the covering graphs where one of the elementary subgraphs has only internal propagators.

We can first begin by showing that if we have two matrices $\boldsymbol{M}_1$ of degree d_1 and $\boldsymbol{M}_2$ of degree d_2, then the covering graphs involved in $\mathrm{Tr}((\boldsymbol{M}_1 - \mathbb{E}(\boldsymbol{M}_1))\boldsymbol{M}_2)$ are the covering graphs of $\mathrm{Tr}(\boldsymbol{M}_1\boldsymbol{M}_2)$ minus the ones where the propagators are internal. Let's denote the color of the open edge by l. To distinguish the $d_1 + d_2$ vertices and their indices, we assign numbers to each vertex. Namely the vertices of $\boldsymbol{M}_1$ are denoted by $1, \ldots, d_1$ with 1 and 2 associated to the two vertices adjacent to the open edge of $\boldsymbol{M}_1$, and $d_1, \ldots, d_1 + d_2$ where the vertices of the open edge of $\boldsymbol{M}_2$ are $d_1 + 1$, $d_1 + 2$.

We denote all the indices by a, and the indices of all colors associated to a vertex l by $a_l^{\mathcal{D}}$.

A subset of the symmetric group $\sigma(d_1 + d_2)$ are the permutations which could be written as $\tau_1\tau_2$ where τ_1 is a permutation of $(1, \ldots, d_1)$ and τ_2 is a permutation of $(d_1, \ldots, d_1 + d_2)$.

We denote by the symbol $\delta_{aa}^{\mathcal{B}}$ the δ of all the indices that are contracted in the graph.

Let $\mathcal{B}_1$ the graph associated to $\boldsymbol{M}_1$ and $\mathcal{B}_2$ the graph associated to $\boldsymbol{M}_2$.

Let $\mathcal{B}'$ the subgraph of $\mathcal{B}$ obtained by opening an edge of color c corresponding to the vertices i and j, it is an elementary subgraph of $\mathcal{B}^r$, the graph corresponding to $\mathrm{Tr}(M^r)$. We have

$$\mathbb{E}(\boldsymbol{M}_1)_{ij} = \delta_{a_1{}^l, i} \delta_{a_2{}^l, j} \sum_{\substack{a \\ a \neq a_1{}^l, a_2{}^l}} \delta_{aa}^{\mathcal{B}_1} \sum_{\tau \in \mathfrak{S}(d_1)} \prod_{l=1}^{d_1} \delta_{a_l{}^{\mathcal{D}} a_{\tau(l)}^{\mathcal{D}}}, \tag{27}$$

$$\mathbb{E}(\mathrm{Tr}(\boldsymbol{M}_1\boldsymbol{M}_2)) = \sum_a \delta_{aa}^{\mathcal{B}} \sum_{\tau \in \mathfrak{S}(d_1+d_2)} \prod_{l=1}^{d_1+d_2} \delta_{a_l{}^{\mathcal{D}} a_{\tau(l)}^{\mathcal{D}}}, \tag{28}$$

Since the edges of $\mathcal{B}$ are the union of the edges of $\mathcal{B}_1$ and $\mathcal{B}_1$ and an edge of color l connecting the vertices of the open edges: 1 with $d_1{+}1$ and 2 with $d_1{+}2$, we have: $\delta_{aa}^{\mathcal{B}} = \delta_{aa}^{\mathcal{B}^1} \delta_{aa}^{\mathcal{B}^2} \delta_{a_1^l, a_{d_1+1}^l} \delta_{a_2^l, a_{d_1+2}^l}$. This let us write:

$$\mathbb{E}(\mathrm{Tr}((\boldsymbol{M}_1 - \mathbb{E}(\boldsymbol{M}_1))\boldsymbol{M}_2)) = \sum_a \delta^{\mathcal{B}}_{aa} \Bigg[\sum_{\tau \in \mathfrak{S}(d_1+d_2)} \prod_{l=1}^{d_1+d_2} \delta_{a_l{}^{\mathcal{D}} a^{\mathcal{D}}_{\tau(l)}} - \sum_{\tau_1 \in \mathfrak{S}(d_1), \tau_2 \in \mathfrak{S}(d_2)} \prod_{l=1}^{d_1} \delta_{a_l{}^{\mathcal{D}} a^{\mathcal{D}}_{\tau_1(l)}} \prod_{m=d_1+1}^{d_1+d_2} \delta_{a_m{}^{\mathcal{D}} a^{\mathcal{D}}_{\tau_2(m)}} \Bigg], \tag{29}$$

Thus the only permutations that are not cancelled are the permutations that does not live invariant the subset $\{1, \dots, d_1\}$, which means that $\exists i \in \{1, \dots, d_1\}$ such that $\tau(i) \in \{d_1 + 1, \dots, d_1 + d_2\}$. These permutations correspond to the covering graphs that does not have only internal propagators connecting the vertices of $\boldsymbol{M}_1$. This proves our claim.

Proof of lemma 11 :

The idea of the proof is that if we assume that an intermediate graph $\mathcal{G}^{\text{int}}$ gives the largest contribution for $\beta \geq \beta_{\text{dec}} = n^{k/4}$, then we can construct a covering graph for the pure noise graph that has a largest contribution than $\mathcal{G}^{\text{int}}$, which is a contradiction.

Let $\mathcal{G}$ a graph whose detection algorithm has $\beta_{\text{dec}} = n^{k/4}$ as a detection threshold. This means that either one of the intermediate graphs or the pure signal graph has a contribution much larger than the contribution of the pure noise graph.

Let's assume that an intermediate graph $\mathcal{G}^{\text{int}}$ (with r vertices replaced by spikes) has the largest contribution for $\beta > \beta_{\text{dec}}$. Let's take the covering graph of $(\mathcal{G}^{\text{int}})^2$ that is responsible for the largest contribution.

We build a covering graph for the pure noise graph from this covering graph. To do so, we disconnect the propagators from the vertices having a spike and connect them together (in any way we want), while we connect by a new propagator each vertex of spike to its equivalent in the mirror graph. This covering graph will give a strictly superior contribution to the expectation if the graph is connected since:

- The cycles that didn't involve a spike stay give the same contributions
- The cycles that involved a spike were giving a contribution equal to one in addition to the β^r direct contributions of the spikes. But in the new covering graph of the pure noise graph, the contribution these cycles will be n^α with $\alpha > 3r/4$.

Thus for $n^{3/4} \ll \beta \ll n^\alpha$, the pure noise graph has a larger contribution than the intermediate graph, which leads to a contradiction.

The demonstration for the matrices $\boldsymbol{M}$ follows the same steps but instead of $\mathcal{G}^2$, one has to consider $\mathrm{Tr}(\boldsymbol{M}^r)$.